Where are the most ancient stars in the Milky Way?

Kareem El-Badry,[1]★ Joss Bland-Hawthorn,[2,3,4] Andrew Wetzel,[5] Eliot Quataert,[1] Daniel R. Weisz,[1] Michael Boylan-Kolchin,[6] Philip F. Hopkins,[7] Claude-André Faucher-Giguère,[8] Dušan Kereš[9] and Shea Garrison-Kimmel[7]

[1]*Department of Astronomy and Theoretical Astrophysics Center, University of California Berkeley, Berkeley, CA 94720, USA*
[2]*Miller Institute, University of California Berkeley, Berkeley, CA 94720, USA*
[3]*Centre of Excellence for All Sky Astrophysics in 3 Dimensions (ASTRO-3D), Sydney, NSW 2006, Australia*
[4]*Sydney Institute for Astronomy, School of Physics, University of Sydney, Sydney, NSW 2006, Australia*
[5]*Department of Physics, University of California, Davis, CA 95616, USA*
[6]*Department of Astronomy, The University of Texas at Austin, Austin, TX 78712, USA*
[7]*TAPIR, Mailcode 350-17, California Institute of Technology, Pasadena, CA 91125, USA*
[8]*Department of Physics and Astronomy and CIERA, Northwestern University, Evanston, IL 60208, USA*
[9]*Department of Physics, Center for Astrophysics and Space Sciences, University of California at San Diego, La Jolla, CA 92093, USA*

ABSTRACT

The oldest stars in the Milky Way (MW) bear imprints of the Galaxy's early assembly history. We use FIRE cosmological zoom-in simulations of three MW-mass disc galaxies to study the spatial distribution, chemistry, and kinematics of the oldest surviving stars ($z_{\rm form} \gtrsim 5$) in MW-like galaxies. We predict the oldest stars to be less centrally concentrated at $z = 0$ than stars formed at later times as a result of two processes. First, the majority of the oldest stars are not formed *in situ* but are accreted during hierarchical assembly. These *ex situ* stars are deposited on dispersion-supported, halo-like orbits but dominate over old stars formed *in situ* in the solar neighbourhood, and in some simulations, even in the galactic centre. Secondly, old stars formed *in situ* are driven outwards by bursty star formation and energetic feedback processes that create a time-varying gravitational potential at $z \gtrsim 2$, similar to the process that creates dark matter cores and expands stellar orbits in bursty dwarf galaxies. The total fraction of stars that are ancient is more than an order of magnitude higher for sight lines *away* from the bulge and inner halo than for inward-looking sight lines. Although the task of identifying specific stars as ancient remains challenging, we anticipate that million-star spectral surveys and photometric surveys targeting metal-poor stars already include hundreds of stars formed before $z = 5$. We predict most of these targets to have higher metallicity ($-3 < [{\rm Fe/H}] < -2$) than the most extreme metal-poor stars.

Key words: Galaxy: evolution – Galaxy: formation – Galaxy: stellar content.

1 INTRODUCTION

The oldest stars in the Milky Way (MW) are relics of star formation in the early Universe, providing a probe of physical processes that can otherwise be studied only at high redshift (e.g. Freeman & Bland-Hawthorn 2002; Beers & Christlieb 2005; Frebel & Norris 2015). Determining the properties, phase–space distribution, and stellar yields of first- and second-generation stars is therefore a primary goal of near-field cosmology (e.g. Abel, Bryan & Norman 2000; Bromm & Larson 2004; Karlsson, Bromm & Bland-Hawthorn 2013; Frebel & Norris 2015). Ongoing spectroscopic

and photometric surveys of the Galaxy have already begun to identify large numbers of metal-poor stars suspected to be ancient (e.g. Beers, Preston & Shectman 1985; Christlieb 2003; Helmi et al. 2003; García Pérez et al. 2013; Yong et al. 2013; Schlaufman & Casey 2014; Casey & Schlaufman 2015; Howes et al. 2015, 2016; Li et al. 2015; Minniti et al. 2016; Cescutti, Chiappini & Hirschi 2017; Starkenburg et al. 2017b), and parallel efforts to measure precise atmospheric parameters, masses, ages, and detailed abundance patterns for large samples of these stars are underway (e.g. Rauer et al. 2014; Li et al. 2015; Ricker et al. 2015; Feltzing et al. 2017; Fernández-Alvar et al. 2017; Sharma et al. 2018).

Given the archaeological interest in identifying very old stars, there arise the questions of (a) where, in terms of both physical location and metallicity, ancient stars can most efficiently be found,

★ E-mail: kelbadry@berkeley.edu

and (b) how metallicity and age are correlated for old stars. Numerous studies have shown that the MW's stellar halo and satellite galaxies retain a wealth of information about the Galaxy's assembly history and earliest stellar populations (e.g. Bullock, Kravtsov & Weinberg 2001; Bullock & Johnston 2005; Salvadori, Schneider & Ferrara 2007; Helmi 2008; Kirby et al. 2008; Bovill & Ricotti 2011; Brown et al. 2014; Beniamini, Dvorkin & Silk 2018; Magg et al. 2018). The observational fact that the stellar halo consists primarily of metal-poor stars broadly supports this notion. On the other hand, cold dark matter (CDM) simulations predict that the number density of old stars should be highest near the Galactic centre, in the bulge and innermost stellar halo ($r \lesssim 3$ kpc; e.g. White & Springel 2000; Brook et al. 2007; Gao et al. 2010; Salvadori et al. 2010; Tumlinson 2010; Starkenburg et al. 2017a; Griffen et al. 2018). Due to efficient enrichment in regions of high star formation rate density at early times, ancient stars found in the inner Galaxy are predicted to be more metal-rich than those in the outer halo ($r \gtrsim 20$ kpc).

The search for ancient and metal-poor stars has a long observational history.[1] Metal-poor RR Lyrae stars were identified in the bulge and inner stellar halo nearly a century ago (Baade 1946, 1951) and were subsequently associated with first- and/or second-generation stars (Walker & Terndrup 1991; Soszyński et al. 2011; Minniti et al. 2016). The kinematics of metal-poor halo stars were used by Eggen, Lynden-Bell & Sandage (1962) in an early attempt to constrain the MW's formation history. Wallerstein et al. (1963) proposed to use the abundance patterns of metal-poor halo giants to constrain Galactic chemical enrichment models.

More recently, the search for ancient stars has targeted ultra metal-poor (UMP) stars ([Fe/H] $\lesssim -4$; e.g. Keller et al. 2014; Aguado et al. 2018) and somewhat higher metallicity stars ([Fe/H] < -2) with *r*-process enhancement. UMP stars are of particular interest because they are diagnostic of the yields of first-generation stars (Beers & Christlieb 2005; Karlsson et al. 2013; Norris et al. 2013; Bessell et al. 2015); in some cases, their abundance patterns appear consistent with enrichment by a single supernova. However, they are quite rare: only a few dozen stars have been identified with [Fe/H] < -4 (Frebel & Norris 2015; Starkenburg et al. 2017a), making a statistical study of the population challenging. It also remains unclear whether UMP stars are unambiguously ancient, as many theoretical models predict them to continue forming in low-density environments until relatively late times (until $z = 2-3$; White & Springel 2000; Brook et al. 2007; Tornatore, Ferrara & Schneider 2007; Trenti, Stiavelli & Michael Shull 2009).

Metal-poor stars with enhanced *r*-process elements and no detectable or weak *s*-process enrichment are thought to have formed at an early time before the onset of the asymptotic giant branch (AGB) phase (likely $\lesssim 300$ Myr after the formation of the first stars; Hill et al. 2002; Frebel & Norris 2015; Ji et al. 2016; Hansen et al. 2017; Ji & Frebel 2018). A few such stars have measured radioactive lifetimes that indicate that they are very old (Sneden et al. 1996; Cayrel et al. 2001; Frebel et al. 2007; Hill et al. 2017), albeit with systematic uncertainties. *r*-process enhanced metal-poor stars have been identified in the bulge, in the stellar halo, and in Local Group dwarf galaxies.

In this work, we study the oldest stars in *simulated* galaxies with the goals of making predictions for MW surveys and better understanding the origin of the oldest stars already being observed. We focus on three $L_\star$ disc galaxies from the FIRE project[2] with z

$= 0$ observable properties that are broadly consistent with the MW. We first present the properties of the oldest stars at $z = 0$ and then trace the stars back to their formation sites, quantifying the effects of accretion stars formed *ex situ* and outward migration of stars formed *in situ* on the distribution of all old stars at $z = 0$.

Many previous theoretical works (e.g. Scannapieco et al. 2006; Salvadori et al. 2007, 2010; Gao et al. 2010; Komiya et al. 2010; Tumlinson 2010; Ishiyama et al. 2016; Griffen et al. 2018) have predicted the $z = 0$ spatial distribution of old stars in MW-like galaxies using simple analytic prescriptions for the formation sites of ancient stars combined with dark-matter-only simulations or Monte-Carlo merger trees based on Press–Schechter theory. These works have all predicted old stars to be centrally concentrated at $z = 0$ because the earliest stellar generations are predicted to form in the highest density peaks, and these preferentially end up near the centre of the primary halo by $z = 0$; i.e. in the bulge. Some studies (Brook et al. 2007; Sharma, Theuns & Frenk 2017; Starkenburg et al. 2017a) have also arrived at similar conclusions using cosmological hydrodynamics simulations including star formation and cooling.

In this work, we study the formation and subsequent evolution of ancient stars in cosmological zoom-in simulations that (a) self-consistently include the effects of baryonic feedback, (b) explicitly model a multiphase interstellar medium (ISM), leading to bursty star formation at high redshift and in low-mass haloes, and (c) produce realistic MW-like galaxies at $z = 0$. As we will show, baryonic feedback processes arising from bursty star formation have non-negligible effects on the late-time distribution of old stars. In particular, we find that feedback-driven fluctuations in the gravitational potential at high redshift drive old stars that are formed near the galactic centre outward, into the outer bulge and inner stellar halo. This effect has not been captured by previous studies of ancient stars, which have either ignored the effects of baryons altogether or have adopted a simplified model of the ISM that suppresses the burstiness of star formation (see further discussion in Section 5).

The remainder of this paper is organized as follows. In Section 2, we introduce the FIRE simulations. In Section 3, we show the predicted spatial, chemical, and kinematic distributions of the oldest stars at $z = 0$. In Section 4, we wind back the clock and identify the formation sites for the oldest stars. In Section 5, we compare our results to earlier work. We summarize our findings in Section 6 and discuss prospects for identifying the surviving population of ancient stars in ongoing MW surveys. In Appendix A, we examine how sensitive our results are to changes in mass resolution and in the turbulent diffusion coefficient.

2 FIRE SIMULATIONS

We study cosmological zoom-in simulations of three MW-mass galaxies from the FIRE project (Hopkins et al. 2014). The simulations were run with the GIZMO[3] hydrodynamics code (Hopkins 2015) in the Lagrangian 'meshless finite mass' mode, using the FIRE-2 model for galaxy formation and feedback (Hopkins et al. 2017a). For details regarding the physical processes modelled in these simulations and their numerical implementation, we refer to Hopkins et al. (2017a,b). The three haloes we study were first presented by Wetzel et al. (2016) and Hopkins et al. (2017a). Their properties are summarized in Table 1. At $z = 0$, they host galaxies

---

[1] For a full history, see Sandage (1986), and references therein.
[2] See the FIRE project website at http://fire.northwestern.edu.

[3] A public version of the GIZMO code is available at http://www.tapir.caltech.edu/~phopkins/Site/GIZMO.html.

Table 1. Summary of simulations.

Name	$\log(M_{\text{star}})$ (M$_\odot$)	$\log(M_{\text{200m}})$ (M$_\odot$)	$f_{z_{\text{form}}>5}$	$f_{[\text{Fe/H}]<-2}$	$f_{z_{\text{form}}>5,\,\|}$ $[\text{Fe/H}]<-2$	m_{b} (M$_\odot$)	m_{DM} (M$_\odot$)
m12i	10.8	12.1	0.0009	0.0063	0.12	7070	35200
m12f	10.9	12.2	0.0029	0.0031	0.49	7070	35200
m12m	11.1	12.2	0.0011	0.0031	0.26	7070	35200

Note: M_{star} is the stellar mass within $3 \times R_{1/2}$, where $R_{1/2}$ is the 3D stellar half-mass radius. M_{200m} is the total mass within R_{200m}, where R_{200m} is the radius within which the matter density is $200 \times$ the mean matter density. M_{star} and M_{200m} are reported at $z = 0$. $f_{z_{\text{form}}>5}$ and $f_{[\text{Fe/H}]<-2}$ are the fraction of stars within 10 kpc at $z = 0$ that formed before $z = 5$ and have $[\text{Fe/H}] < -2$, respectively. $f_{z_{\text{form}}>5|[\text{Fe/H}]<-2}$ is the fraction of stars with $[\text{Fe/H}] < -2$ that formed before $z = 5$. The last two columns show m_{b} and m_{DM}, the average baryon and dark matter particle masses.

with structural parameters broadly similar to the MW. They have realistic stellar discs and bulge-to-disc ratios (Garrison-Kimmel et al. 2017a; El-Badry et al. 2018b), HI rotation curves and velocity dispersions (El-Badry et al. 2018a), satellite populations (Wetzel et al. 2016; Garrison-Kimmel et al. 2018), and stellar haloes (Bonaca et al. 2017; Sanderson et al. 2017).

Although the three simulated galaxies have similar gross structural properties at $z = 0$, we will show in Section 4 that their early assembly histories differ from one another substantially, as is common in CDM (Cooper et al. 2010). Given that we do not currently identify a clear reason to prefer one simulated MW-analogue over another, we view the three simulations as realizations of plausible assembly histories that could produce a MW-like galaxy at $z = 0$. Without firmer priors on the formation history of the MW, the scatter between the simulations sets a lower limit on the uncertainty of our predictions as applied to the real MW.

Due to significant uncertainties in the properties and formation process of zero-metallicity stars (see e.g. Bromm & Larson 2004; McKee & Tan 2008; Wise et al. 2012; Bromm 2013), the FIRE model does not attempt to explicitly model Pop III stars. Instead, the abundances of all baryon particles in the simulation are set to a metallicity floor of $[\text{M}_i/\text{H}] = -4$ in the initial conditions, where $[\text{M}_i/\text{H}]$ denotes the logarithmic abundance of individual metal species compared to their Solar value. The specific value of the metallicity floor is somewhat arbitrary; a floor is required to prevent numerical problems in cooling, and $[\text{M}_i/\text{H}] = -4$ is similar to the typical value expected after enrichment by Pop III stars (Bromm & Yoshida 2011; Bland-Hawthorn, Sutherland & Webster 2015). Different metallicity floors have been used elsewhere in the literature (e.g. Starkenburg et al. 2017a), but systematic studies of the effects of varying the metallicity floor on the formation sites of ancient stars have yet to be carried out and represent a promising avenue for future work. The first generation of stars formed in the simulation quickly enrich the surrounding gas, so that most stars formed after $z \sim 10$ are enriched to $[\text{M}_i/\text{H}] \sim -3$, a factor of 10 enhancement over the metallicity floor. The metallicity floor is therefore not expected to significantly bias the abundances of these stars; nevertheless, we caution against overinterpreting the abundances of the most metal-poor stars in the simulation $[\text{M}_i/\text{H}] \lesssim -3.5$.

The realizations of the simulations studied in this work, unlike the first realization presented in Wetzel et al. (2016), were run with the subgrid model for turbulent diffusion of metals described in Hopkins et al. (2017a), using a diffusion coefficient $C_0 \approx 0.003$. Although the inclusion of turbulent metal diffusion has a negligible effect on galaxies' overall structural properties, including total metallicity (Hopkins et al. 2017a; Su et al. 2017), it has been shown to improve metal mixing in the ISM and produce more realistic metal-

licity distribution functions, particularly preventing the unphysical formation of very low-metallicity stars at late times (Escala et al. 2018; Wetzel et al., in preparation). We explore the model's sensitivity to the choice of diffusion coefficient in Appendix A. There we show that our results are relatively insensitive to the choice of diffusion coefficient, though the properties of the most ancient stars ($z_{\text{form}} \gtrsim 7$) do vary somewhat with simulation resolution.

Each star particle in the simulation represents a simple stellar population with fixed abundances, uniform age, and a typical initial mass of 7070 M$_\odot$. For a metal-poor, 13 Gyr-old stellar population with a Kroupa (2001) initial mass function (IMF), every 1000 M$_\odot$ of $z = 0$ stellar mass in old star particles represents roughly 15 giant and subgiant stars (each with $m \approx 0.8\text{M}_\odot$), which are the primary targets of spectroscopic surveys of the MW.[4]

3 OLD STARS AT LATE TIMES

3.1 Spatial distribution

Fig. 1 shows the spatial distribution and fractional contribution to the total stellar mass of old stars in our simulations. The left-hand panels show projections of a single galaxy, m12i, as viewed by an observer in the solar circle; i.e. in the disc mid-plane, 8.2 kpc from the galaxy's centre. In the top three panels, we include all stars within a distance $r < 30$ kpc of the galaxy's centre; in the bottom panel, we consider a survey centred on the solar neighbourhood and extending to a distance of 10 kpc.

In the second left-hand panel of Fig.1, we show the projected sky distribution for stars that were born before $z = 5$ (1.2 Gyr after the Big Bang in our adopted cosmology), which we refer to as 'old' or 'ancient' stars.[5] Here, we simply plot each old star particle as a single pixel, but we remind the reader that each particle represents an entire stellar population with initial mass ~ 7000 M$_\odot$, containing of order 100 giant and subgiant stars. Consistent with expectations

---

[4]Because their ages are easier to constrain, the number of RR Lyrae stars is also potentially of interest. The frequency of RR Lyrae stars and its dependence on metallicity is poorly constrained, but a rough estimate based on measurements of GCs and nearby dwarf galaxies (Sherwood & Plaut 1975; Harris 1996; Baker & Willman 2015) is 1 RR Lyrae star per 10^4M$_\odot$ in $z = 0$ old ($\gtrsim 10$ Gyr) stellar mass; i.e. 1 ancient RR Lyrae for every 150 ancient giants and subgiants.

[5]We note that the cut of $z_{\text{form}} > 5$ primarily yields stars younger than the oldest 'population 2.9' stars sought by UMP star surveys, some of which may have formed as early as $z = 20-30$ (Frebel & Norris 2015); however, we find no significant differences between the spatial distribution and kinematics of the first stars formed in the simulation at $z = 15-20$ and those forming at $z = 5$.
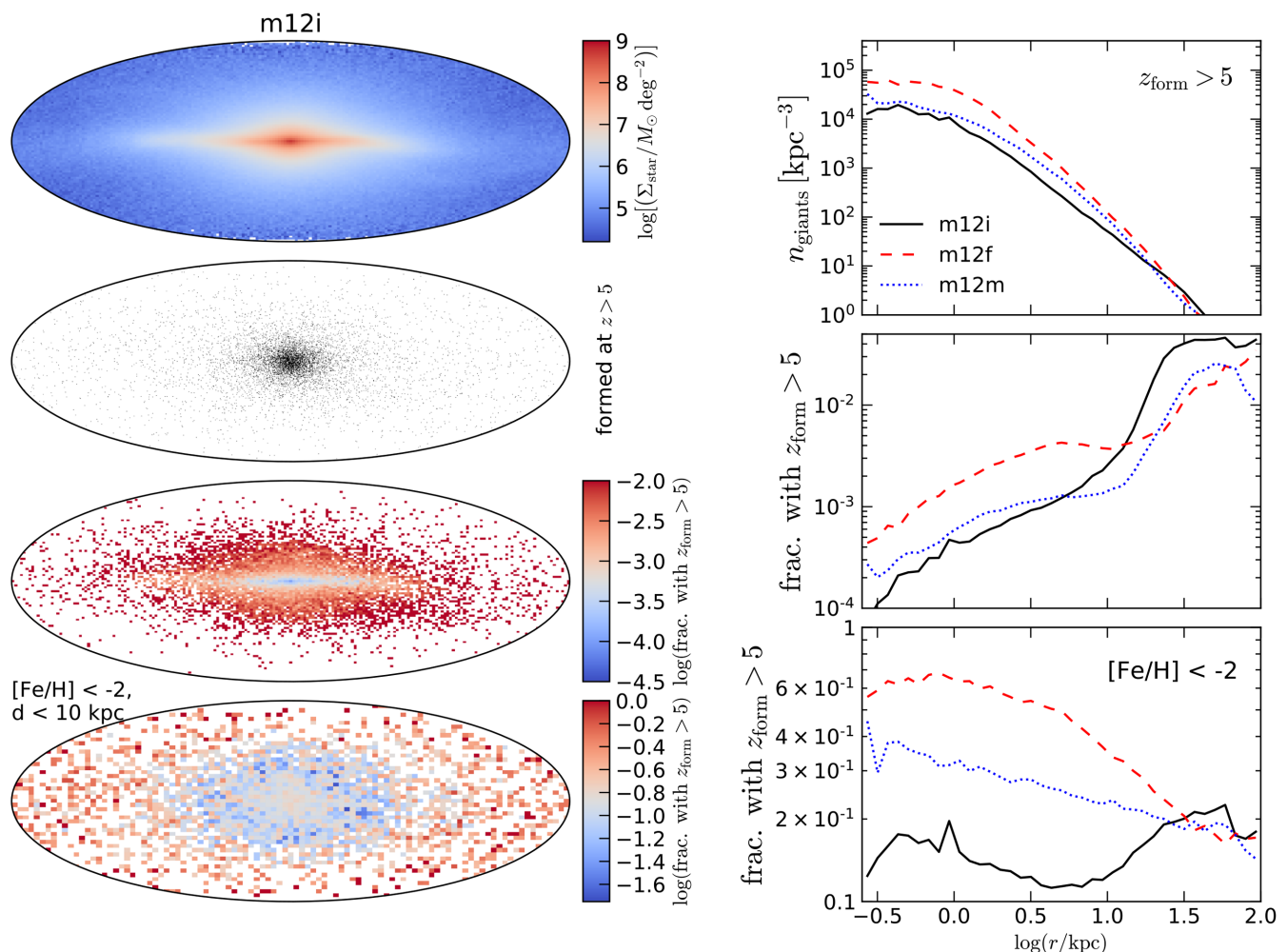
Figure 1. **Left**: Aitoff projections of the m12i simulation for an observer in the disc mid-plane at the solar circle ($r = 8.2$ kpc). We show the integrated surface density of all stars today (top) and the spatial distribution of stars formed before $z = 5$ (second panel). Because the oldest stars are distributed in a uniform spheroid extending to large radius, while later-forming stars are concentrated in the disc and central bulge, the fraction of all stars along a given line of sight that are old is *lowest* for sightlines towards the galactic centre (third panel). Bottom panel shows fraction of stars with [Fe/H] < -2 within 10 kpc of the solar neighborbood that are ancient. **Right**: Giant number density (top) and total mass fraction (middle) of old stars in three simulated MW-like galaxies. In all three galaxies, the total number density of old stars is highest near the galactic centre, but old stars are less centrally concentrated than stars formed at later times, so old stars make up a larger fraction of the total population at large radii, in the stellar halo. Bottom panel shows the fraction of metal-poor stars that are ancient; this varies only weakly with radius but is generally highest in the inner galaxy.

from previous work (e.g. White & Springel 2000; Bland-Hawthorn & Peebles 2006; Brook et al. 2007), this panel shows that the absolute number of old stars found in a particular line of sight is largest towards the dense inner regions of the galaxy. However, the total surface density of all stars – most of which formed at later times – is also highest towards the inner galaxy. The third panel on the left-hand side of Fig. 1 shows that as a result the fraction of ancient stars increases substantially as a function of radius, particularly for sight lines out of the galactic plane.

In the bottom left-hand panel of Fig. 1, we predict the returns of a bright magnitude-limited survey targeting metal-poor stars. We consider only star particles within 10 kpc of the solar neighbourhood, which we place at an arbitrary azimuth on a circle of radius $r = 8.2$ kpc in the disc mid-plane. 10 kpc corresponds roughly to the maximum distance at which an old, metal-poor giant can be detected by current MW spectroscopic surveys (e.g. GALAH or APOGEE, with magnitude limits of V$\approx$14; De Silva et al. 2015;

Majewski et al. 2017).[6] We then show the fraction of all stars with [Fe/H] < -2 along a given sight line that are old ($z_{form} > 5$). Considering only metal-poor[7] stars removes most of the substructure due to the bulge and disc seen in the upper panels, as most bulge and disc stars in the simulated galaxies formed later ($z \gtrsim 1 - 2$) and have higher metallicities (Ma et al. 2017). The bottom left-hand panel shows that in m12i, the total fraction of stars that are ancient is lower towards the galactic centre even when metal-rich stars are

---

[6]Our result are not sensitive to the distance limit of 10 kpc; increasing it slightly lowers the fraction of metal-poor stars that are ancient, as the outer halo contains more metal-poor stars formed at later times.

[7]Unless otherwise stated, we use 'metallicity' to refer specifically to [Fe/H]. For the Solar abundances, we adopt $12 + \log(n_{Fe}/n_H) = 7.50$ and (later in text) $12 + \log(n_{Mg}/n_H) = 7.60$ from Asplund et al. (2009), where n_X denote number densities.

discarded. However, the opposite is true in m12f and m12m (bottom right-hand panel).

In the right-hand panels of Fig.1, we show the 3D absolute number density and fractional mass contribution of ancient stars for all three simulated galaxies. In the top panel, we approximate the number of red giant stars contributed by every old star particle; here, we assume a Kroupa (2001) IMF and use the MIST isochrones (Choi et al. 2016) for old, metal-poor stars that were used by El-Badry, Weisz & Quataert (2017a). In the middle and bottom panels, we plot the fraction of all stellar mass (middle) and of star particles with [Fe/H] < −2 (bottom) that are ancient. Two qualitative trends in the distribution of old stars are similar for the three simulations: their absolute number density is highest near the galactic centre, while the fraction of all stars that are old is highest in the outer halo. In detail, there are non-trivial differences between the simulations. The total number of old stars is higher by a factor of ∼5 in m12f than in m12i; despite this, the fraction of stars in the outer halo that are old is higher in m12i. When only iron-poor star particles are considered, the fraction of stars that are ancient increases with radius in m12i and decreases in m12m and m12f. We explore these differences further in Section 4.

The absolute number of giants with $z_{\rm form} > 5$ predicted within 10 kpc of the solar neighbourhood in the three simulations is (0.6, 2.3, and 1.2) $\times 10^6$ for m12i, m12f, and m12m, respectively. For $z_{\rm form} > 10$, the corresponding numbers are (1.8, 7.0, and 6.3) $\times 10^4$. We note that we have made no attempt to account for extinction, source confusion, or survey selection functions. Forthcoming mock catalogues for the three simulated galaxies studied here (Sanderson et al. 2018) will make it possible to do so.

3.2 Metallicity

Many ongoing searches for the oldest stars in the MW operate under the implicit assumption that the oldest stars are also the most metal-poor. We now investigate the relation between metallicity and age predicted by our simulations.

Fig. 2 shows the age–[Fe/H] relation of stars that occupy the central 10 kpc of the m12i simulation at $z = 0$ (see Lamberts et al. 2018 for the age–metallicity relation for all metals). Qualitatively, most ancient stars are metal-poor, and most metal-poor stars are old. However, it is also clear that particularly for old stars, the relationship between age and [Fe/H] is not monotonic. For example, selecting stars with [Fe/H] = −2 yields stars formed between $z \sim 8$ and $z \sim 1.5$, and stars with $z_{\rm form} \sim 5$ have $-3 \gtrsim$ [Fe/H] $\gtrsim -1$.

In the right-hand panel of Fig. 2, we show for all three simulations the fraction of metal-poor stars within 10 kpc of the solar neighbourhood that formed before a given redshift. For all three simulated galaxies, the majority of stars with [Fe/H] < −2 formed before $z = 2.5$; the redshift at which half of nearby metal-poor stars had formed is $z = 4-5$, while the redshift at which 10 per cent had formed is $z = 6-8$. Thus, we predict that selecting stars with [Fe/H] < −2 in a survey of the inner Galaxy will yield stars with median formation redshifts of ∼5, with of order 10 per cent forming before reionization.

The right-hand panel of Fig. 2 also highlights the non-trivial effects of the details of MW-like galaxies' different early assembly histories on the age distributions of their oldest stars at $z = 0$: the fraction of metal-poor stars that formed before a particular redshift varies by a factor of ∼6 between the earliest (m12f) and latest (m12i) forming galaxies.

In Fig. 3, we investigate the metallicity distributions of stars of different ages in more detail. The left-hand panel shows the metal-

licity distribution for four different formation redshift intervals. Most stars formed before $z = 10$ have [Fe/H] < −3, while most stars with $5 < z_{\rm form} < 10$ have [Fe/H] < −2. The most common metallicity for stars in the latter interval is [Fe/H] ∼ −2.4, but the distribution is quite broad. ∼20 per cent of stars with $z_{\rm form} > 5$ have [Fe/H] < −3. The vast majority of stars formed at late time are enriched to higher metallicities: essentially all stars formed after $z = 1$ have [Fe/H] > −1.

Fig. 3 also shows that nearly 70 per cent of stars with $z_{\rm form} > 10$ (and 4 per cent of those with $5 < z_{\rm form} < 10$) have [Fe/H] = −4; i.e. they formed from gas that had not been enriched above the metallicity floor at all. These metallicities clearly cannot be interpreted literally; fortunately, the majority of stars formed after $z \sim 8$ are enriched above this level. The latest-forming star particles that are in the central 10 kpc at $z = 0$ and have pristine abundances form at $z = 4.3$ (m12i), $z = 4.1$ (m12f), and $z = 3.5$ (m12m).

The right-hand panel shows the distribution of formation redshifts in bins of metallicity. Very low-metallicity stars with [Fe/H] < −3 form over a broad range of redshifts, peaking at $z \sim 4$. There are roughly equal numbers of stars with metallicities above and below [Fe/H] = −3 at $8 < z_{\rm form} < 10$. The more enriched population begins to dominate at later redshifts, outnumbering the extremely metal-poor population by a factor of ∼10 at $z = 5$ and >100 at $z = 3$. Conversely, metal-rich stars are almost never ancient: Only ∼0.1 per cent of stars formed before $z = 5$ have [Fe/H] > −1.

We do not show abundance distributions for elements other than iron, but we also find that all old stars that have been enriched above the metallicity floor exhibit enhanced abundance of α elements (e.g. Mg and Si) relative to solar values. Star particles formed before $z \sim 3$ typically have [α/Fe] ~ 0.4, while those forming after $z = 1$ typically have [α/Fe] $\lesssim 0.25$. Enhancement in α elements is a necessary but not sufficient condition for a star particle to be ancient in our simulations: Typical [α/Fe] values do not begin to drop until $z \sim 3$ in all three simulations. Detailed abundance tracks for the simulated galaxies studied here will be presented in Wetzel et al. (in preparation).

3.3 Kinematics

We now examine the kinematics of old stars in our simulated galaxies and compare to the kinematics of the populations formed at later times. Fig. 4 shows Toomre diagrams for stars in m12i, separating all stars, stars in a range of decreasing metallicity bins, and the oldest stars. For consistency with work on the kinematics of stars in the MW solar neighbourhood, we select stars in a cylindrical shell centred on $R = 8$ kpc; however, our results do not depend sensitively on the region in which stars are selected. The Toomre diagram compares the azimuthal rotation velocity of stars (V_ϕ) with the speed along axes perpendicular to the main rotational motion. We define the cylindrical coordinate system such that the $+\hat{z}$ axis is aligned with the net stellar angular momentum vector.

The upper left-hand panel of Fig. 4 shows all stars. Most stars are in the disc, rotating coherently with mean rotation velocity $\langle V_\phi \rangle \sim 230 \, {\rm km \, s^{-1}}$. There is also a non-rotating, dispersion-supported population centred on $\langle V_\phi \rangle \sim 0$ that contains <10 per cent of the total stellar mass for stars near the solar circle. Stars in this region of the Toomre diagram are typically referred to as having 'halo-like' orbits. We refer to Bonaca et al. (2017) for further discussion of stellar kinematics in the solar neighbourhood of this simulation and comparison to observations of the MW.

The upper middle panel shows only metal-rich stars, and the following three panels show stars in increasingly lower [Fe/H] bins.
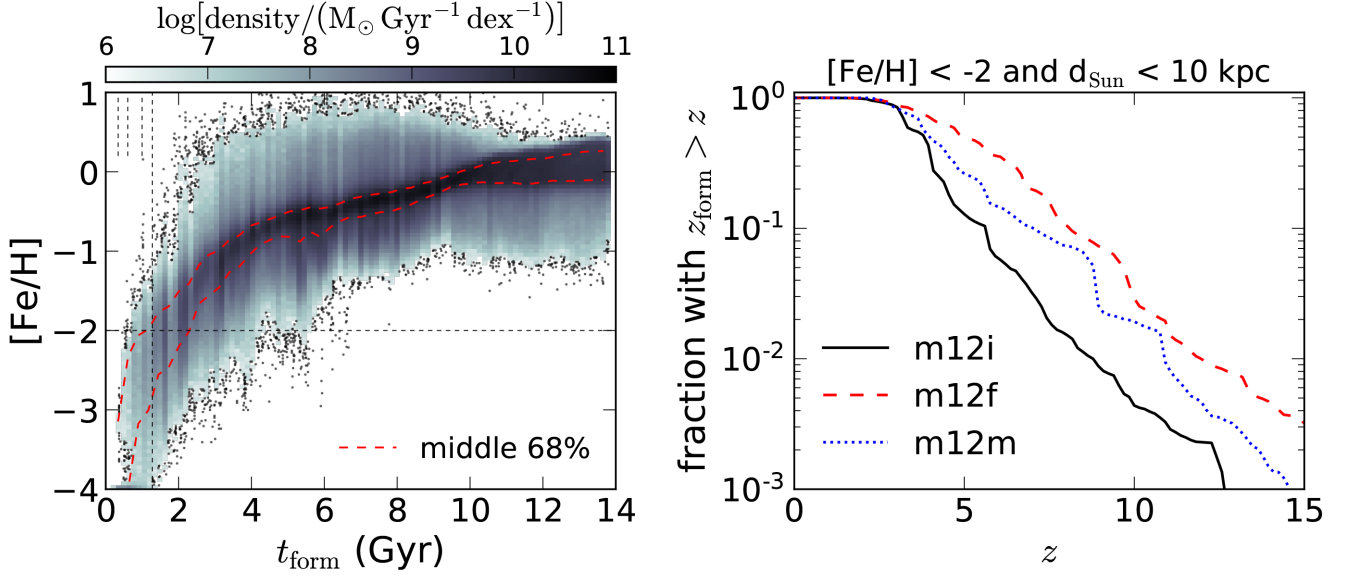
Figure 2. **Left**: Age–[Fe/H] relation for all stars within the central 10 kpc of the m12i simulation. Vertical overdensities correspond to coherent bursts of star formation. Dashed vertical lines show $z = 10, 8, 6, 5$, from left to right. Stars forming at $z = 5$ have a broad range of iron abundances, with $-4 < [Fe/H] < -1.5$; stars with $[Fe/H] = -2$ continue to form past $z = 2$. **Right**: Cumulative fraction of stars with $[Fe/H] < -2$ and a distance $d < 10$ kpc from the solar neighbourhood that formed before redshift z, for all three simulated galaxies in our sample. Depending on the details of the MW's formation history, we predict that $0.5-3$ per cent of metal-poor stars within 10 kpc of the solar neighbourhood formed before $z = 10$ and $10-50$ per cent formed before $z = 5$.
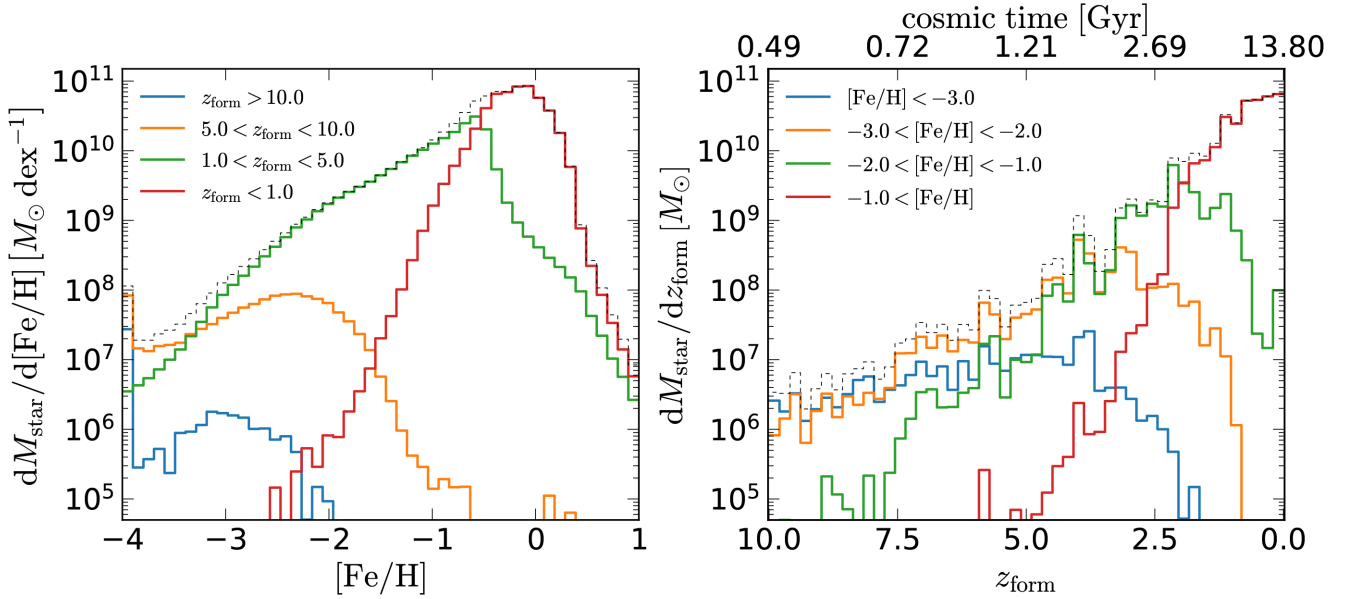
Figure 3. **Left:** Distribution of stellar metallicities and formation redshifts for stars in the central 10 kpc of the simulation m12i at $z = 0$. The coloured histograms show individual metallicity/formation redshift bins; the dashed black histogram shows total for all stars. Early-forming stars ($z_{form} \gtrsim 5$) exhibit a broad range of metallicities peaked at $-3 < [Fe/H] < -2$; they constitute ~ 10 per cent of all stars with $[Fe/H] < -2$ and almost half of all stars with $[Fe/H] < -3$. **Right:** Stars with $[Fe/H] > -3$ dominate over extremely metal-poor stars at $z_{form} \gtrsim 8$; for $z_{form} = 5$, there are a factor of ~ 10 more stars with $[Fe/H]$ above -3 than below.

Most stars with $[Fe/H] > -1$ are in the rotation-supported disc population, while most stars that are more metal-poor are found on dispersion-supported orbits. This occurs because the disc in our simulated galaxies forms at $z \sim 1$ (Ma et al. 2017),[8] when

---

[8]We note that the onset of disc formation is gradual, and its timing varies somewhat across our simulated galaxies (Garrison-Kimmel et al. 2017a). We remain agnostic of the precise age of the MW's disc.
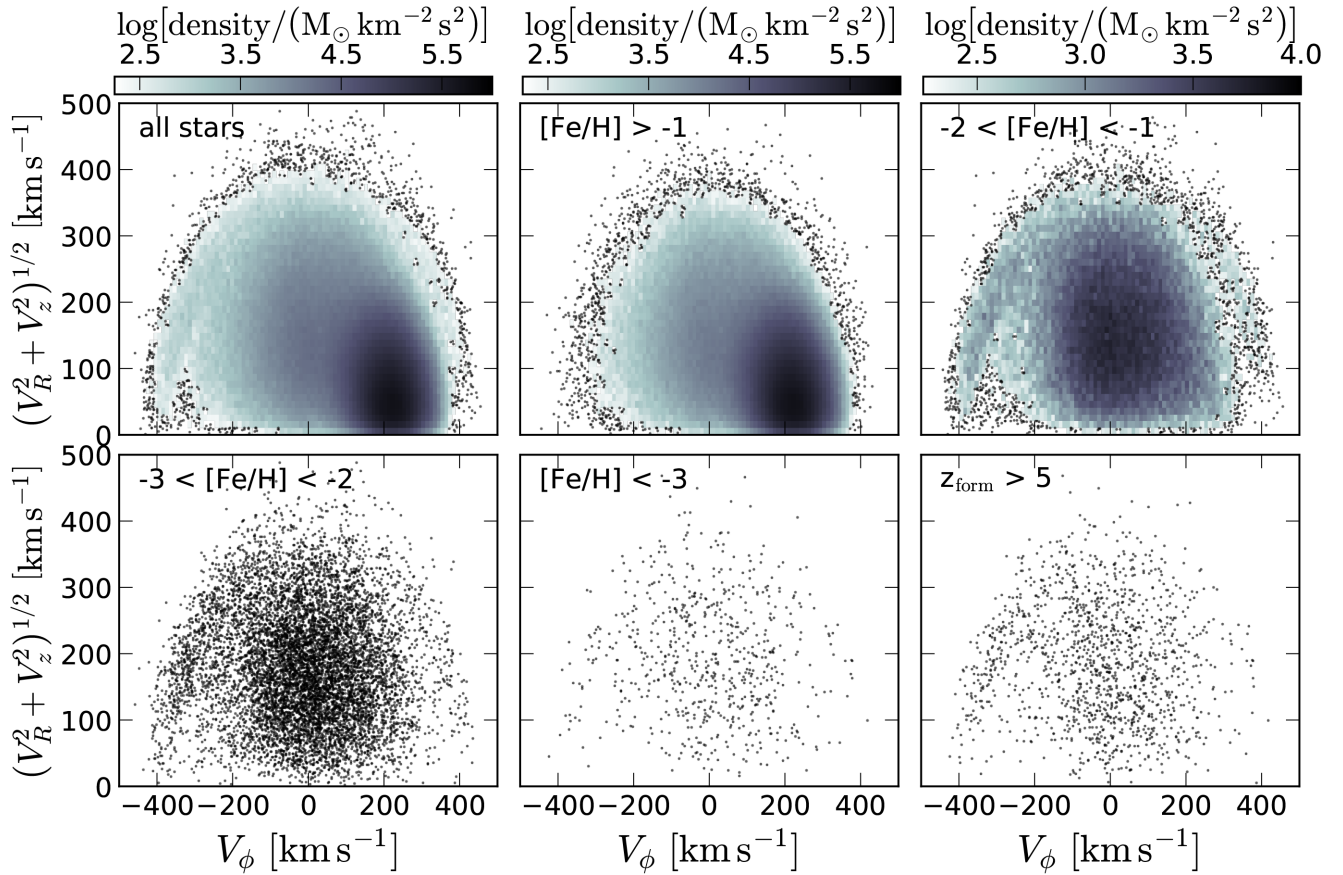
the mean iron abundance was $[Fe/H] \sim -0.8$ (see Fig. 2). Some substructure due to disrupted satellites can be seen in the Toomre diagrams for metal-poor stars, but there is little systematic difference between the kinematics of stars with $-2 < [Fe/H] < -1$ and those with $-3 < [Fe/H] < -2$ or $[Fe/H] < -3$. Similarly, selecting only old stars ($z_{form} > 5$; bottom right-hand panel) yields dispersion-supported orbits indistinguishable from those of metal-poor stars formed at later times (before $z \sim 1$, after which most stars form in the

Figure 4. Toomre diagrams of stars in the solar circle of the m12i simulation at $z = 0$. We select stars in a cylindrical shell with $6 < R/\text{kpc} < 10$ extending $\pm 2\,\text{kpc}$ from the disc mid-plane and plot all stars, stars in a range of decreasing metallicity bins, and stars that formed before $z = 5$. In the top three panels, we plot density as a colour scale when more than five star particles fall within a given pixel. Most stars in the solar neighbourhood are found on rotation-supported, disc-like orbits, but almost all of these stars have $[\text{Fe/H}] > -1$. Metal-poor stars inhabit primarily dispersion-supported orbits. All old stars are dispersion-supported, with no significant coherent rotation.

disc). Having dispersion-supported kinematics is thus a necessary but not sufficient condition for a star in the simulated galaxies being ancient.

We find qualitatively similar results for the m12f and m12m simulations: The vast majority of the oldest stars are found on dispersion-supported orbits, but at fixed galactocentric radius, there is little difference between the kinematics of the oldest stars and stars formed at intermediate redshifts.

4 WHERE DID THE OLDEST STARS FORM?

We have shown that the FIRE simulations predict the oldest stars in MW-like galaxies to be less centrally concentrated than later-forming stars, extending from the galactic centre into the outer halo (Fig.1, middle right-hand panel). Previous works (e.g. El-Badry et al. 2016; Anglés-Alcázar et al. 2017; Bonaca et al. 2017; Sanderson et al. 2017) have shown that mergers and secular dynamical processes, particularly outflow-driven fluctuations in the gravitational potential, can cause stars to migrate substantially after they form. We now investigate where the oldest stars formed, and how they arrived at their present-day spatial and kinematic distribution.

4.1 Defining formation sites

To determine where the oldest stars in the simulated galaxies at $z = 0$ formed, we tag star particles that formed before $z = 5$ and are in the primary galaxy at $z = 0$ (unless otherwise stated, within 10 kpc of the galactic centre) and then trace them back to the time of their formation. For each old star particle, we calculate the distance (always in physical units) from the main progenitor galaxy at the time of the star particle's formation, which we approximate as the first simulation output in which it appears.[9] We determine the main progenitor in each snapshot as follows.

At $z = 0$, the main galaxy in the zoom-in region is identified as the galaxy with the highest stellar mass that is uncontaminated by lower resolution dark matter particles. Its centre is located using an iterative 'shrinking-spheres' method (Power et al. 2003), wherein we recursively compute the centre of mass of star particles in a spherical region, reducing the sphere's radius by ~50 per cent and re-centring on the new stellar centre of mass at each iteration.

---

[9]Simulation outputs are saved every ~20 Myr, so star particles are expected to migrate ≪1 kpc on average (with respect to their host galaxy at formation) between their formation and the first snapshot in which their positions are saved.

We then trace the main galaxy back through all simulation outputs. We define the main progenitor in terms of stellar mass, not halo mass. In each output, we first calculate the 'expected' location of the galaxy at that time by extrapolating backwards from its position and velocity in the next snapshot. We then repeat the shrinking-spheres centring algorithm, beginning with a sphere of radius 20 kpc centred on the expected location. We define the galaxy identified in this way as the 'main progenitor' in each output.

This procedure ensures that the same galaxy is followed consistently through all snapshots. At high redshift, it is often the case that the main progenitor is not the most massive galaxy in the zoom-in region since different galaxies grow at different rates. To ensure that the method produces the desired behaviour, we also verify that for every simulation output, more than 50 per cent of the star particles in the main progenitor were also in the main progenitor in the previous output. We note that due to scatter in the $M_{star}-M_{halo}$ relation, the main progenitor identified in this way is not necessarily the same as the main progenitor identified from the dark matter merger tree (e.g. Fitts et al. 2018).[10]

4.2 *In situ* versus *ex situ* formation

In Fig. 5, we trace the oldest stars in the m12i simulation back to their locations at high redshift. The left-hand panel shows the spatial distribution at $z = 5$ of star particles that inhabit the central 10 kpc of the galaxy at $z = 0$. It is clear that at $z = 5$, these stars were *not* part of a single coherent population but were distributed throughout of order 100 distinct lower mass galaxies that subsequently merged. In m12i, the main progenitor (shown in the centre of the left-hand panel of Fig. 5) *was* already the most massive galaxy in the zoom-in region, but it still contained less than half of the old stars that would make their way into the central galaxy by $z = 0$. We note that many of the dark matter haloes in the left-hand panel of Fig. 5 that do not contain red points *do* host stars; they simply never merge with the main progenitor and are swept up in the Hubble flow by $z = 0$.

The right-hand panel of Fig. 5 shows the distance from the main progenitor of stars that formed before $z = 5$ at the time of their formation (i.e. some time before $z = 5$; red) and at $z = 0$ (black). We plot distributions of formation distance for stars within different concentric shells at $z = 0$. The dotted red histogram shows that, even considering only stars in the central 10 kpc at $z = 0$, a majority of old stars formed at distances of order 100 kpc from the main progenitor. When stars in the outer halo at $z = 0$ are included (solid red line), only a few per cent of the oldest stars formed in the main progenitor. The most distant-forming stars in the central 10 kpc at $z = 0$ formed at distances of ~250 kpc, while some stars in the outer halo formed at distances in excess of 400 kpc from the main progenitor.

Comparing the black and red histograms in the right-hand panel of Fig.5, it is also evident that old stars that formed in the central regions of the main progenitor have on average moved to larger distance by $z = 0$. We investigate this in more detail in Section 4.3.

Fig. 6 shows explicitly how the fraction of stars formed *ex situ* (which we define as forming more than 20 kpc from the main progenitor) varies with formation time. In the top panel, for m12i only, we show the *ex situ* fraction in different radial bins. At all formation

---

[10]We find that defining the main progenitor using star particles generally yields the same results as when dark matter particles are used at low redshift, but not at $z \gtrsim 3$. At very high redshifts ($z \gtrsim 10$), it can even occur that the main progenitor defined from the dark matter merger tree does not contain any stars.
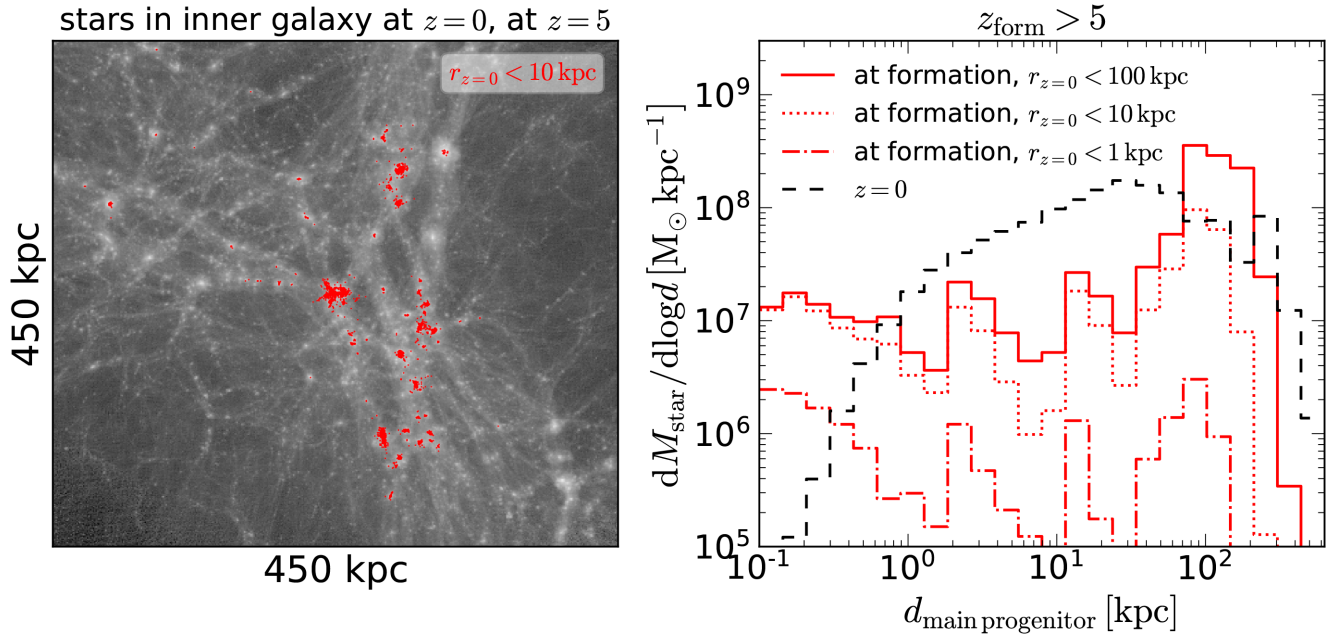
redshifts, the *ex situ* fraction increases monotonically with radius: more centrally concentrated stars were preferentially formed *in situ*. However, even for the central bin ($r_{z=0} < 10$ kpc), in m12i it is only after $z = 2$ that stars formed *in situ* begin to dominate over those accreted at later times. Intriguingly, this panel also shows that a non-zero fraction of stars in the outer halo ($30 < r_{z=0}$/kpc < 100), including some formed at late times, formed *in situ*. We find that these stars primarily form from already-outflowing, feedback-driven gas clouds, similar to results found in other simulations (Purcell, Bullock & Kazantzidis 2010; Cooper et al. 2015; Elias et al. 2018). The origin and fate of these stars will be explored in more detail by Yu et al. (in preparation).

The bottom panel of Fig. 6 compares the fraction of stars within 10 kpc at $z = 0$ that formed *ex situ* in all simulations. For all three simulated galaxies, at least half of the stars born before $z \sim 4$ were formed *ex situ* and subsequently accreted. However, the fraction of stars of a given age formed *ex situ* varies substantially across the three simulations: in m12m, *ex situ* stars dominate at $z_{form} > 2$, while in m12f, of order half of all stars formed *in situ* up to $z = 10$.

Fig. 7 shows the fraction of stars formed *ex situ* as a function of metallicity rather than formation redshift. Even within the solar circle, most metal-poor stars formed *ex situ* and were subsequently accreted. The metallicity below which the majority of stars in the inner galaxy formed *ex situ* varies between -1.9 in m12f and -1.2 in m12m. This suggests that simply selecting metal-poor stars – at any radius – will predominantly yield stars that formed *ex situ*.

In Fig. 8, we show the spatial distribution at $z = 0$ of the oldest stars in all three simulations, separating stars that formed *in situ* and those that formed *ex situ*. Old stars formed *in situ* are generally more centrally concentrated: in m12i, they outnumber the *ex situ* stars in the central ~1 kpc, but *ex situ* stars become dominant at $r > 5$ kpc. The situation is qualitatively similar in m12f, which formed earlier, but *in situ* stars make up a larger fraction of the old population and thus dominate out to ~5 kpc. Finally, in m12m, the *ex situ* population is completely dominant at all radii.

In m12m, the main progenitor does not contribute the oldest coherent population of old stars in the galaxy, as several other haloes host galaxies more massive than the main progenitor at $z \sim 5$ that eventually merge with the main progenitor. In this sense, 'main progenitor' is not an especially meaningful title at high redshift: although the main progenitor can always be uniquely defined, there is no guarantee that it is the *dominant* progenitor. Similarly, the distinction between *in situ* and *ex situ* stars ceases to be physically meaningful before a main progenitor is established.

In Fig. 9, we consider the possibility of distinguishing between the *in situ* and *ex situ* populations based on $z = 0$ observables. Here, we show the simulation m12f, which has a coherent main progenitor up to the highest redshifts and thus offers the best chance of exhibiting a coherent *in situ* population at late times. Consistent with previous work (Johnston et al. 2008; Corlies et al. 2013), we find that the mean metallicity of old stars is higher for the old *in situ* population, reflecting the fact that the galaxy mass–metallicity relation remains steep at high redshift (Ma et al. 2016). It is thus in principle possible to assign a known old star a probability of having formed *in situ* based on its metallicity; for example, an old star in m12f with [Fe/H] $= -1.5$ has a >90 per cent probability of having formed *in situ*. In practice, separating the *in situ* and *ex situ* populations based on [Fe/H] alone is entirely infeasible, both due to the difficulty of reliably age dating such moderately low-metallicty stars and because the metallicity distributions of the MW's old *in situ* and *ex situ* stars are not known a priori. We discuss possible

Figure 5. **Left**: The red points show the oldest stars in the main galaxy in the `m12i` simulation – i.e. stars within 10 kpc of the galactic centre at $z = 0$ – traced back to $z = 5$. The greyscale shows the projected dark matter surface density, integrated over a 400 kpc column. All units are physical, not comoving. At $z = 5$, the main progenitor (centre of left-hand panel) contains less than half of the old stars that will end up in the inner galaxy by $z = 0$. **Right**: Distances of the oldest stars from the main progenitor galaxy's centre at the time of their formation (red) and at $z = 0$ (black). The majority of the oldest stars in the galaxy at $z = 0$ did not form there but were deposited later through mergers. Stars in the outer halo at $z = 0$ formed at even larger distances on average than those in the inner regions; the opposite is true for stars in the central 1 kpc.
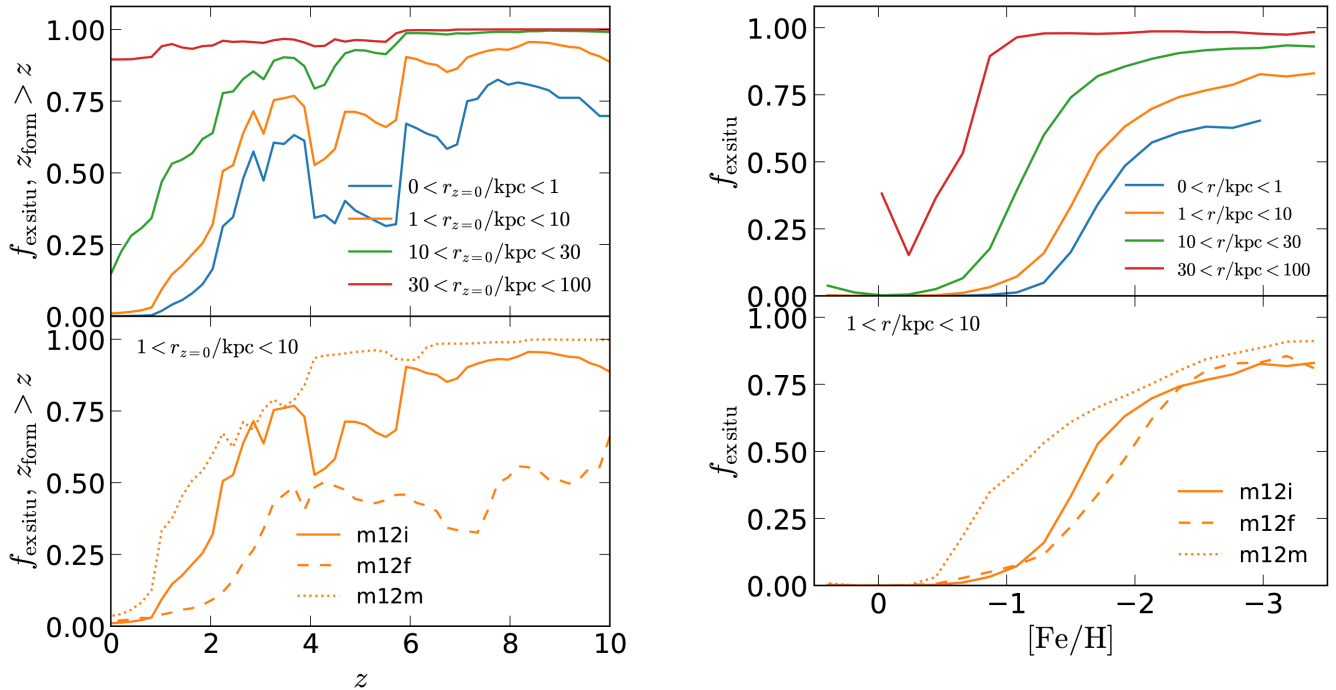
Figure 6. **Top**: Cumulative fraction of stars forming before redshift z that formed *ex situ* (i.e. more than 20 physical kpc from the main progenitor) in `m12i`. We plot stars in different radial bins at $z = 0$ separately. The fraction of stars formed *ex situ* increases with $r_{z=0}$ for stars of all ages. Most stars with $z_{\rm form} \gtrsim 3$ – even those in the inner galaxy at $z = 0$ – formed *ex situ*. **Bottom**: Same, but for all three simulated galaxies, considering a single radial bin. *Ex situ* stars generally dominate the population formed before $z \sim 3$, but there is significant variation in the detailed formation histories of the three simulations.
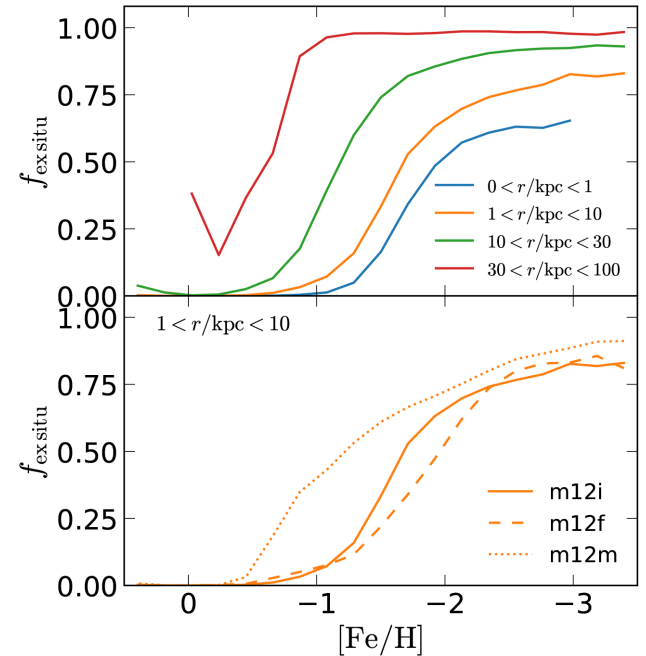
Figure 7. **Top**: Fraction of stars with a given metallicity that formed *ex situ* and were subsequently accreted in `m12i`. We plot stars in different radial bins at $z = 0$ separately. The fraction of stars formed *ex situ* increases with r for stars of all metallicities. Most stars with $[\rm Fe/H] \lesssim -1.5$ – even those in the inner galaxy – formed *ex situ*. **Bottom**: Same, but for all three simulated galaxies, considering a single radial bin. *Ex situ* stars dominate the low-metallicity population in all simulations.
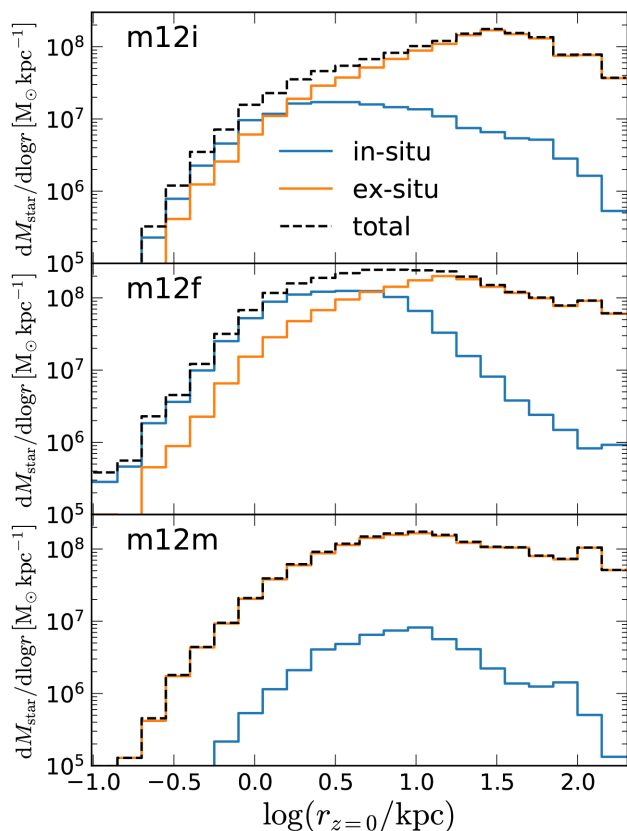
Figure 8. Radial distribution of old stars ($z_{\mathrm{form}} > 5$) at $z = 0$ for all three simulated MW-like galaxies. Stars formed *in situ* are generally more centrally concentrated than those formed *ex situ*; they dominate over *ex situ* stars in the central $\sim$1 kpc (m12i) and $\sim$5 kpc (m12f). In m12m, the main progenitor contained only a small fraction of the total stellar mass at $z > 5$, so *ex situ* stars dominate at all radii.

avenues for distinguishing these populations based on abundances of other elements in Section 6.

In the right-hand panel of Fig. 9, we compare Toomre diagrams of the old *in situ* and *ex situ* populations in m12f. Contours are separated by factors of 2 and show the velocity–space surface density of old stars, normalized by the total mass of each population. This figure shows that the *in situ* and *ex situ* populations have essentially indistinguishable kinematics: both are dispersion supported and retain no obvious memory of their formation. This is perhaps unsurprising since violent relaxation during hierarchical merging at later times generously redistributes energy between stellar orbits. Bonaca et al. (2017) found similar results for stars in the solar neighbourhood of m12i, including those formed and accreted at later times. Similarly, Sanderson et al. (2017) found *ex situ* and *in situ* stars in these simulated galaxies to be spatially co-located and well mixed at $z = 0$, such that standard attempts to separate the populations using photometric profiles perform poorly.

Our simulations predict that a large fraction of the oldest stars in the MW – including those near the centre today – did not form locally but were accreted at later times after forming in external subhaloes. This in part explains why our model predicts a reduced fraction of old stars towards the Galactic centre (Fig. 1) and overwhelming dispersion-supported kinematics for old stars (Fig. 4): while stars that form at later times ($z \lesssim 2$) are born from low-orbital energy gas near the centre of the primary halo's gravitational potential, stars deposited in mergers have higher energies and are spread

over a large range of radii (e.g. Bullock & Johnston 2005; Sharma et al. 2017).

But as we discuss next, this is only part of the story.

4.3 Outward migration of old stars

It is evident from the right-hand panel of Fig. 5 that stars move both inward and outward between their formation and $z = 0$. As discussed in the previous section, inward motion is a necessary result of hierarchical assembly through mergers. We now investigate in more detail what drives stars to move outward after they form; to this end, we focus on stars formed *in situ* near the galactic centre.

To assess how old stars migrate as a function of redshift, we tag star particles that are near the galactic centre ($r < 5$ kpc) at some high redshift z_{initial}, follow them to $z = 0$, and measure $\Delta r = r_{z=0} - r_{z=z_{\mathrm{initial}}}$ (so outward migration corresponds to positive Δr). Because stellar orbits are not necessarily circular, some non-zero Δr is expected simply due to random changes in orbital phase from one snapshot to the next. To minimize the scatter due to this effect, we always calculate both $r_{z=0}$ and $r_{z=z_{\mathrm{initial}}}$ in five simulations snapshots spread over $\sim$100 Myr; for each particle, we use the median radius over these five snapshots.

We show values of Δr for $z_{\mathrm{initial}} = 5$, 3, and 1 in Fig. 10. The left-hand panel shows distributions of Δr for star particles in m12i. Most stars have moved outwards since $z = 5$, with a median $\Delta r = 2.5$ kpc and $\sim$25 per cent of stars migrating outwards more than 6 kpc. Since $z = 3$, most stars have migrated outwards, but typical Δr values are slightly lower than since $z = 5$. Finally, most stars within $r < 5$ kpc migrate *inwards* between $z = 1$ and $z = 0$. The right-hand panel of Fig. 10 shows the median Δr since redshift z for all three simulations. In all cases, stars formed *in situ* before $z \sim 4$ migrate outwards on average by $z = 0$, but the details differ non-trivially across different simulations.

Although Fig. 10 shows how much stars that were near the galactic centre at a given redshift have migrated by $z = 0$, Fig. 11 follows the migration of one particular set of star particles – those that formed *in situ* and are near the galactic centre at $z = 5$ – as a function of time. For all three simulations, old *in situ* stars (on average) migrate outwards continually between $z = 5$ and $z = 1$ and then migrate inwards between $z = 1$ and $z = 0$.

Previous works (e.g. Read & Gilmore 2005; Stinson et al. 2009; Maxwell et al. 2012; El-Badry et al. 2016, 2017b) have shown that in low-mass galaxies, a time-varying gravitational potential, generated primarily by stellar-feedback driven gas outflows, can drive stars formed *in situ* into the stellar halo. This process has also been shown to create cores in low-mass galaxies' dark matter density profiles (Di Cintio et al. 2014; Chan et al. 2015; Oñorbe et al. 2015). It is not generally thought to operate in $L_\star$ galaxies, as it relies on rapid outflows launched by bursty star formation to drive impulsive changes in the depth of the gravitational potential (Pontzen & Governato 2012, 2014). Star formation is typically not bursty at late times in MW–mass galaxies, but it *is* at higher redshift (e.g. Sparre et al. 2017; Faucher-Giguère 2018). Indeed, the shallow potentials of MW progenitors at early times render them susceptible to the same type of feedback-driven net outward stellar migration found by El-Badry et al. (2016) to operate in low-mass galaxies at late times.

Stars cease migrating outwards after $z \sim 2-1$ (right-hand panel of Figs 10 and 11) because fluctuations in the gravitational potential have largely died down by this time: Mass accumulation in the galactic centre due to continued gas inflow deepens the potential until feedback-driven outflows can no longer impulsively evacuate
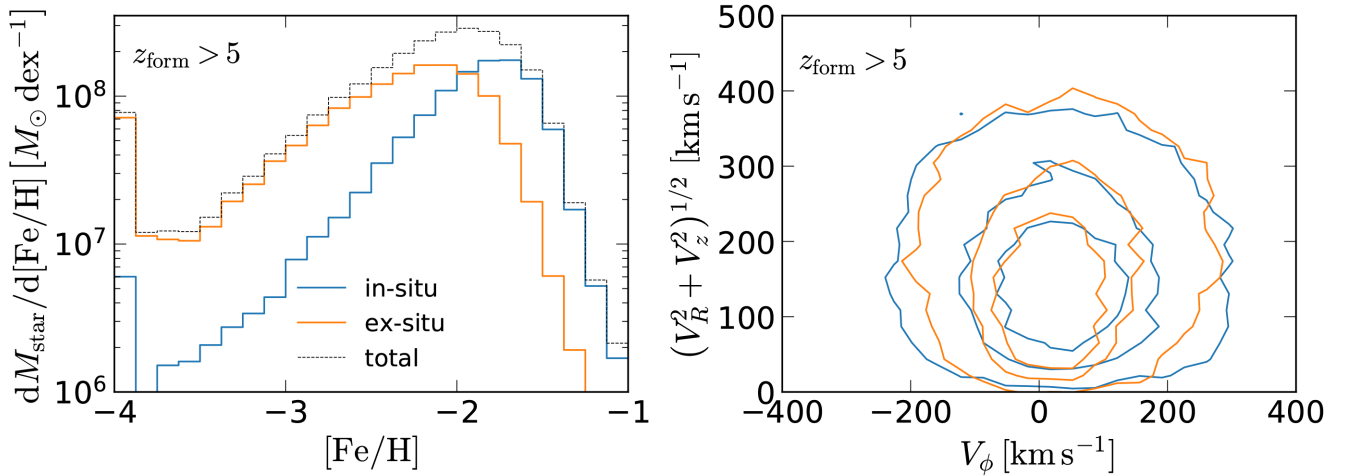
Figure 9. Metallicty distribution (left) and Toomre diagram (right) of old stars in the `m12f` simulation, which has the largest old *in situ* population of the simulations we study (Fig. 8). We divide stars that are in the main galaxy ($r < 30\,\mathrm{kpc}$) at $z = 0$ into *in* versus *ex situ* populations with a distance cut of $d_{\mathrm{main\,progenitor}} = 20\,\mathrm{kpc}$ at the time of their formation. Old stars that formed *in situ* have higher metallicities on average ($\langle[\mathrm{Fe/H}]\rangle = -1.7$) than those that formed *ex situ* ($\langle[\mathrm{Fe/H}]\rangle = -2.2$), but the two populations have identical dispersion-supported kinematics.
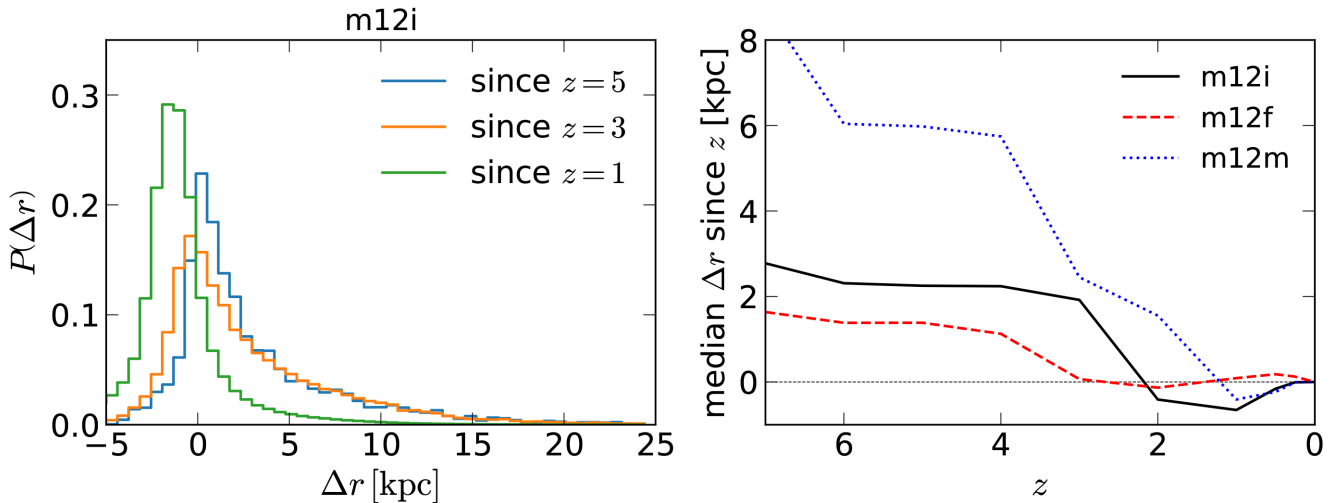
Figure 10. **Left**: Distribution at $z = 0$ of distances stars in the `m12i` simulation have migrated since $z = 5$, $z = 3$, and $z = 1$. At each redshift, we tag all star particles within 5 kpc of the galactic centre and then trace them to $z = 0$, computing $\Delta r = r_{z=0} - r_{z\,\mathrm{initial}}$ (so positive Δr represents outward migration). Fluctuations in the shallow gravitational potential at high redshift can add energy to stellar orbits, causing older stars to migrate to larger radii. These fluctuations have largely died down by $z = 1$, so later-forming stars remain centrally concentrated; in fact, contraction of the central potential during the formation of the bulge causes stars to migrate *inwards* at later times. **Right**: median Δr as a function of time for all three simulations. Outward migration ceases at $z \sim 2-1$ and is weaker for simulations dominated by a single progenitor (see Fig. 6).

dynamically significant quantities of gas from the galactic centre. The stronger (weaker) outward migration of old stars in `m12m` (`m12f`) can also be understood as a consequence of the simulation's less (more) dominant main progenitor at high redshift: it is easier to drive large-scale potential fluctuations, due to both outflows and mergers, in a shallow potential.

After $z \sim 1$, contraction of the potential due to continued accumulation of baryons at high density (e.g. Blumenthal et al. 1986) actually drives stars to migrate *inwards*, partially undoing outward migration at earlier times. This inward migration is somewhat weaker in `m12f`, perhaps because this galaxy forms a weaker bulge than the other two simulations, so that the central potential contracts less at later times (see Garrison-Kimmel et al. 2017a).

Chan et al. (2015) studied the evolution of the central dark matter density profile in FIRE simulation of MW-like galaxies and found

similar redshift evolution to what we find for the oldest stars (e.g. compare Fig. 11 to their fig. 5): stellar feedback-driven potential fluctuations remove dark matter from a galaxy's inner regions until $z \sim 1$, but contraction of the halo at later times due to continued accretion of baryons in the absence of bursty star formation partially undoes this effect by $z = 0$.

5 COMPARISON TO PREVIOUS WORK

A number of previous studies (Scannapieco et al. 2006; Salvadori et al. 2007, 2010; Tumlinson 2010; Ishiyama et al. 2016; Griffen et al. 2018) have used dark matter only simulations combined with semi-analytic prescriptions for the formation sites of the first stars to model the distribution of old stars in MW-like galaxies at $z = 0$. In qualitative agreement with this work, these studies have
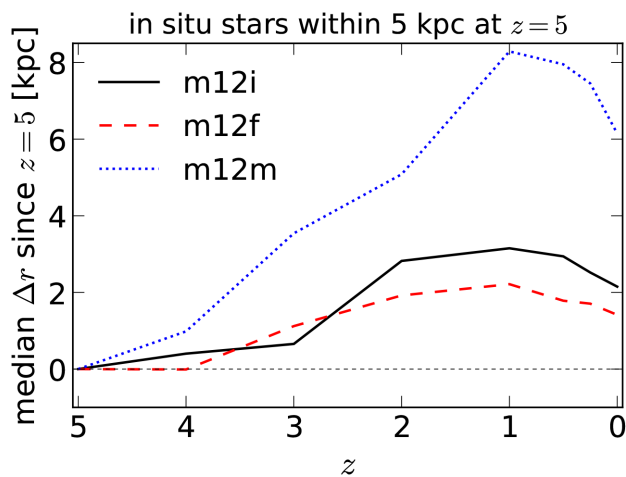
Figure 11. At $z = 5$, we tag star particles with $r < 5$ kpc that formed *in situ*. We then follow the same star particles until $z = 0$, plotting their median outward migration. In all simulations, stars migrate outwards until $z \sim 1$, and then partially migrate back inwards as the potential contracts at $z \lesssim 1$.

predicted old stars to be concentrated near the Galactic Centre. We emphasize, however, that because the population of old stars in the inner galaxy is diluted at $z = 0$ by later-forming stars (by a factor of $\sim$10 000–1; see Fig. 1) it may be more efficient to search for old stars at higher galactic latitudes. We also note that most studies based on dark matter only simulations do not account for destruction of substructure due to the strong tidal field of the baryon overdensity in the inner halo (e.g. Garrison-Kimmel et al. 2017b) and also cannot model baryon-driven fluctuations in the potential that drive stars outwards, so we expect the oldest stars to be somewhat more dispersed than predicted by these works.

Our study most closely resembles the recent work of Starkenburg et al. (2017a), who studied the $z = 0$ distribution of the oldest stars in the APOSTLE simulations (Sawala et al. 2016) of paired haloes selected to resemble the Local Group. These authors found that 50 per cent of the most metal-poor stars, which they defined as [Fe/H] < -2.5, form before $z = 5.3$. We find similar results: for our three haloes, 50 per cent stars with [Fe/H] < -2.5 form before $z = 4.1$ (m12i), $z = 5.0$ (m12f), and $z = 4.8$ (m12m). They find that 90 per cent of the most metal-poor stars form before $z = 2.8$; we find corresponding redshifts $z = 2.8$ (m12i), $z = 2.9$ (m12f), and $z = 3.0$ (m12m).

We also find reasonable agreement with Starkenburg et al. when we reproduce their fig. 2, which shows the fraction of the oldest and most metal-poor stars compared to the total population as a function of galactic radius (see our Fig.1 for a rough comparison); our three haloes all fall within the range of ancient fractions spanned by their simulations. Both APOSTLE and FIRE find that the fraction of the most metal-poor stars that are old declines with radius.

However, the fraction of all stars that are old in the central few kpc is lower than the median value found by Starkenburg et al. (2017a) for all three of our simulated galaxies, by a factor of $\sim$3–4 on average. We also find the fraction of all stars that are ancient to increase by roughly an order of magnitude between the galactic centre and the solar neighbourhood, while they find it to be nearly flat. In other words, old stars in our simulations are less centrally concentrated than in APOSTLE, at least within $r \lesssim 10$ kpc. Similarly, we find that the fraction of metal-poor stars in the inner galaxy is lower by a factor of $\sim$2 in our simulations; this disagreement is somewhat weaker

than that for ancient stars, likely because a significant fraction of the metal-poor stars are formed *ex situ*.

We suspect that old stars in our simulations are less centrally concentrated due to energetic feedback processes that drive outward the stars formed near the centre of the high-redshift MW progenitor's shallow potential. The APOSTLE simulations do not attempt to model cold ($T \ll 10^4$ K) gas and allow star formation to occur at relatively low densities ($n_H \sim 10^{-1}$ cm^{-3}), a factor of 10 000 lower than the star formation density threshold of $n_H = 10^3$ cm^{-3} adopted in the FIRE model. This causes star formation in their simulations to be less-spatially and temporally clustered than in models that attempt to resolve the cold ISM, preventing the formation of cores in the dark matter density profiles of their low-mass galaxies (Oman et al. 2015). Because the mechanism we propose for driving old stars formed *in situ* to larger radii relies in part on the same feedback-driven potential fluctuations that lead to the creation of these cores, we expect it to be less efficient in simulations that do not form cores.

6 SUMMARY AND DISCUSSION

We have studied the spatial distribution, kinematics, metallicity, and formation history of the oldest stars in FIRE cosmological baryonic zoom-in simulations of three MW-mass disc galaxies. Fig. 12 provides a schematic picture of the processes that lead to the observed distribution of the oldest stars at $z = 0$. Our main results are as follows:

(i) *Spatial distribution of old stars at $z = 0$*: The absolute number density of ancient stars ($z_{form} > 5$) is highest near the galactic centre, in the bulge and inner stellar halo. However, because stars that form at later times ($z \lesssim 2$) are *more* centrally concentrated at $z = 0$, the fraction of all stars along a given line of sight that are ancient is in fact *lowest* for sight lines towards the inner galaxy (Fig. 1). The fraction of metal-poor stars that are ancient generally decreases with galactocentric radius but with significant scatter between different simulations.

(ii) *Kinematics of old stars*: The oldest stars in our simulated galaxies are all on dispersion-supported, halo-like orbits, exhibiting no rotational support (Fig. 4). The same is true for most metal-poor stars and most stars formed before $z \sim 1$, so dispersion-supported kinematics are a necessary but insufficient condition for a star to be ancient. Among old stars, stars formed *in situ* (i.e. within the main progenitor) and stars formed *ex situ* (in an external galaxy that was subsequently accreted) have indistinguishable kinematics (Fig. 9).

(iii) *Rapid enrichment*: The first generation of stars formed in the simulations rapidly enrich the gas surrounding their formation sites to [Fe/H] ~ -3, so that a majority of ancient stars have metallicities of $-3 < $ [Fe/H] < -2 (Figs 2 and 3) and enhanced [α/Fe]. Because these moderately low-metallicty stars are more abundant than stars with extremely low metallicity ([Fe/H] < -3), they represent promising targets for surveys attempting to identify the oldest stars in the Galaxy, *if* their ages can be reliably measured. Conversely, the most metal-poor stars are not uniformly old: stars with [Fe/H] < -3 continue to form until $z \sim 3$.

(iv) *In situ versus ex situ formation*: Our simulations predict that a dominant fraction of the ancient stars in the MW at $z = 0$ – even those near the Galactic centre – did not form *in situ* but formed in external galaxies, often more than 100 kpc from the main progenitor, and were deposited in the halo through hierarchical mergers at $5 \lesssim z \lesssim 1$ (Fig. 5). Even in the central 10 kpc, these *ex situ* stars dominate the old, metal-poor population: most stars with $z_{form} \gtrsim 2$ formed *ex*
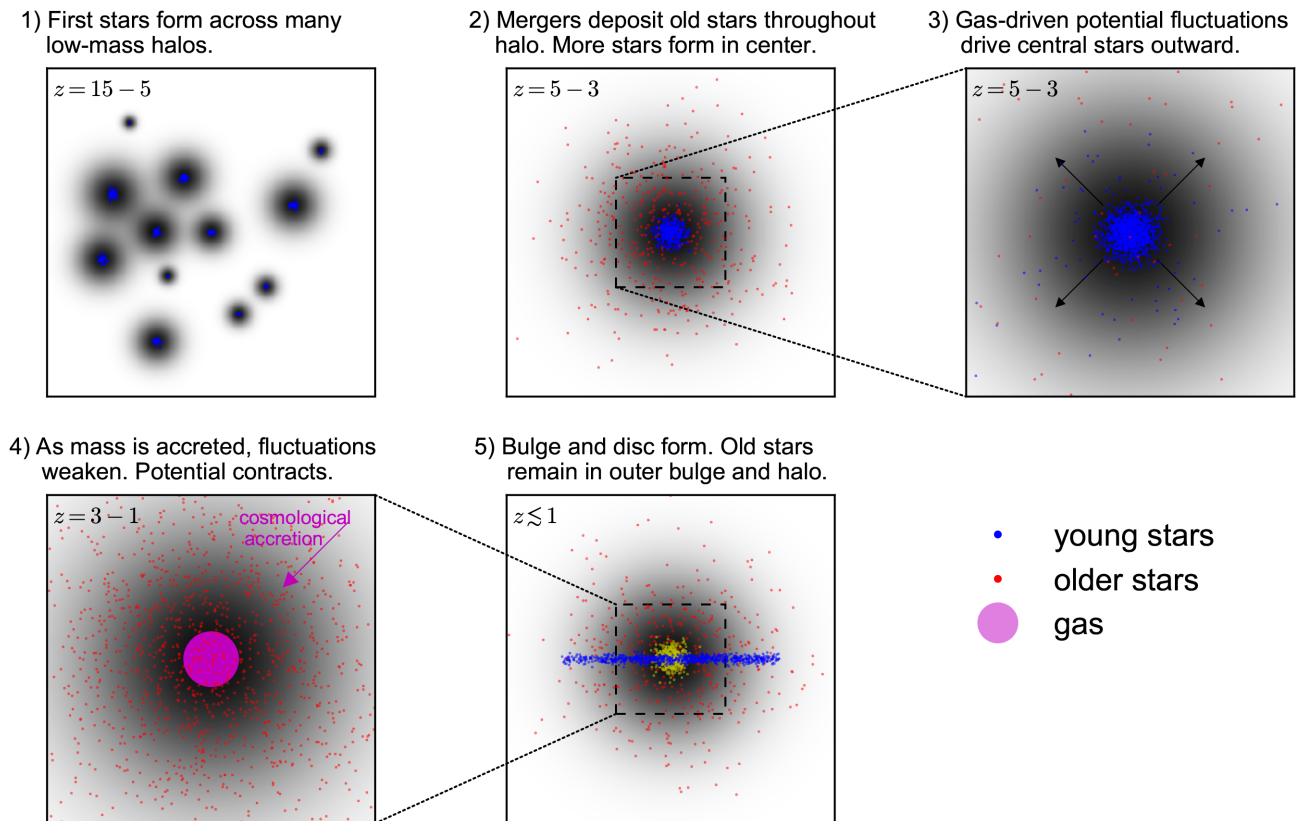
1) First stars form across many low-mass halos.

2) Mergers deposit old stars throughout halo. More stars form in center.

3) Gas-driven potential fluctuations drive central stars outward.

4) As mass is accreted, fluctuations weaken. Potential contracts.

5) Bulge and disc form. Old stars remain in outer bulge and halo.

$z = 15 - 5$

$z = 5 - 3$

$z = 5 - 3$

$z = 3 - 1$ cosmological accretion

$z \lesssim 1$

- • young stars
- • older stars
- ● gas

Figure 12. Schematic illustration of the Galaxy's early assembly. The earliest-forming stars are much less centrally concentrated at late times than stars in the disc and bulge because (a) many are formed *ex situ* and are deposited in the outer proto-halo in mergers, and (b) the oldest stars formed *in situ* are driven to larger radii by outflow-driven fluctuations of the shallow gravitational potential at $z \gtrsim 3$, which couple energy to the orbits of collisionless particles, as in dwarf galaxies.

situ. The same is true for most stars with [Fe/H] $\lesssim -1.5$ (Figs 6 and 7). Accreted stars do not penetrate as deep into the potential as stars formed *in situ* at late times (Figs 5 and 8). This is one of the two primary reasons old stars are less centrally concentrated at $z = 0$ than stars formed at later times.

(v) *Outward migration after formation*: Even old stars that form *in situ* and are initially centrally concentrated migrate outward by $z = 0$. This outward migration is qualitatively similar to the processes proposed to create dark matter cores and drive stars in low-mass galaxies outwards even at later times (El-Badry et al. 2016): fluctuations in the gravitational potential, driven by large-scale gas inflows/outflows as well as mergers, add energy to stellar orbits. These fluctuations die out by $z \sim 2$, so that stars formed at later times do not migrate outwards much and in fact, migrate inwards as the potential contracts at later times (Figs 10 and 11).

6.1 Prospects for identifying the oldest stars

Our simulations predict that a substantial fraction of stars with [Fe/H] $\lesssim -2$ formed before $z = 5$ and are now spread throughout the Galaxy. Magnitude-limited surveys like RAVE, GALAH, APOGEE, LAMOST, and SEGUE find metal-poor stars in abundance. For example, RAVE detected 480 000 stars with SNR > 20 at intermediate spectral resolution ($R \approx 9000$; Kunder et al. 2017), about 6000 of which have $-4 \leq$ [Fe/H] ≤ -2. We expect LAMOST to deliver an even larger set of very metal-poor stars, albeit at lower spectroscopic resolution ($R \approx 2000$; Li et al. 2015). GALAH has observed 550 000 stars to date at high resolution (R

$\approx 30\,000$; De Silva et al. 2015) for which 500 stars with [Fe/H] < -2 have SNR > 50 required for useful measurements of heavy metal abundances. Comparable numbers of metal-poor stars have been observed at high resolution and SNR by APOGEE (Fernández-Alvar et al. 2017; Majewski et al. 2017). *Gaia*–RVS is expected to increase the known population of very metal-poor stars by more than an order of magnitude (Robin et al. 2012).

Photometric surveys have also proved effective for identifying metal-poor stars. Although spectroscopic follow-up is required to measure detailed abundances and kinematics, photometric surveys can reliably identify metal-poor stars more efficiently and at larger distances than spectroscopic surveys, and they are sensitive to dwarfs as well as giants. The fact that metal-poor stars are bluer has long been used to photometrically identify candidate ancient stars (e.g. Wallerstein 1962), and even broad-band photometry (e.g. from SDSS; Ivezić et al. 2008) can yield metallicities accurate at the 0.1 dex level for metal-rich stars ([Fe/H] $\gtrsim -1$). For moderately metal-poor stars ([Fe/H] $\gtrsim -2.5$), intermediate-band Strömgren photometry can reliably measure metallicities with a precision of a few tenth of a dex (Strömgren 1963; Árnadóttir, Feltzing & Lundström 2010). Stars with still lower metallicities can be efficiently identified both with narrow-band photometry targeting the Calcium H&K lines (Beers et al. 1985; Christlieb et al. 2002; Hill et al. 2017; Starkenburg et al. 2017b; Youakim et al. 2017) or mid-infrared photometry targeting broad absorption bands (e.g. Schlaufman & Casey 2014; Casey & Schlaufman 2015). State-of-the-art surveys searching for extremely metal-poor stars can photometrically identify stars with [Fe/H] < -3 with a success rate of up to

∼25 per cent; the majority of their higher metallicity contaminants still have [Fe/H] < −2 (Youakim et al. 2017). Finally, LSST is predicted to find tens of thousands of RR Lyrae stars throughout the Local Group (Oluseyi et al. 2012); these span a wide range of metallicities but are all relatively old ($\gtrsim 10$ Gyr).

Compared to the search for ancient stars at the low-metallicity limit, less effort has been expended to find and study those at $-3 \lesssim$ [Fe/H] $\lesssim -2$. This owes primarily to the difficulty of identifying the oldest members of this population. *If* higher metallicity ancient stars can be reliably identified, targeting them offers some advantages over UMP stars. As we have demonstrated (e.g. Fig. 3), ancient stars with $-3 \lesssim$ [Fe/H] $\lesssim -2$ are predicted to be much more numerous than UMP stars of the same age. At fixed apparent magnitude, more elemental abundances can be measured for stars with higher metallicity, providing a more complete probe of the yields of their progenitor stars and, in exceptional cases, enabling age-dating with more precise chemical clocks. On the other hand, the gas clouds from which more metal-rich ancient stars formed were likely enriched by a larger number of supernovae, so the interpretation of these stars' abundance patterns in terms of first star yields is more challenging.

The most significant challenge facing efforts to use ancient stars for Galactic archaeology stems from the difficulty of measuring accurate stellar ages; i.e. identifying which stars are actually ancient. At present, there is *no* reliable method for age-dating individual old stars with better than ∼10 per cent accuracy (see Soderblom 2010, for a review); this means, for example, that stars formed at $z = 10$ cannot be reliably distinguished from stars formed at $z = 4$, at least not without appealing to galactic chemical enrichment models. Even for Globular Clusters (GCs), where information in many parts of the HR diagram can be leveraged to simultaneously constrain the age of the stellar population, state-of-the-art uncertainties on absolute stellar ages are of order ±1 Gyr (Chaboyer et al. 2017, or see Choksi, Gnedin & Li 2018, for a compilation).

Investments in 3D stellar atmospheric models and measurement of many heavy element abundances (e.g. Nissen et al. 2017; Chiavassa et al. 2018) may somewhat improve age constraints on stars for which exceptionally high-resolution and high-SNR data are available. Measuring accurate stellar ages will nevertheless present a significant challenge for the foreseeable future. This is due in large part to persistent and fundamental uncertainties in stellar interior models, such as shortcomings in mixing-length theory (Joyce & Chaboyer 2017) and non-negligible uncertainties in the experimentally measured opacities used for stellar interior calculations (e.g. Bailey et al. 2015).

Ongoing and planned asteroseismic missions are predicted to deliver mass measurements of some red giant branch (RGB) stars (Chaplin et al. 2014; Rauer et al. 2014; Ricker et al. 2015) accurate enough to, in principle, yield ages that are accurate at the 5−10 per cent level. However, uncertainties in mass-loss rates on the RGB (e.g. Miglio et al. 2012) are currently large enough to prevent measurement of initial stellar masses with better than ∼10 per cent accuracy, and asteroseismic mass estimates for most RGB stars carry similar uncertainties (Stello et al. 2015). Typical uncertainties on asteroseismic ages thus remain of order 15 per cent (Silva Aguirre et al. 2015) comparable to the uncertainties in age estimates of giants from the spectroscopic [C/N] ratio (e.g. Ness et al. 2016) and age estimates for main-sequence stars with white dwarf companions (Fouesneau et al. 2018). The *precision* of such ages is likely to improve with the influx of better data, but the uncertainties in stellar models discussed above currently set a more uncompromising limit on the accuracy of absolute ages, at the 7–10 per cent level. We

also note that asteroseismic mass determinations for low-metallicity stars may be subject to some biases (e.g. Epstein et al. 2014), and precise [C/N]-based ages cannot be obtained at low metallicity.

In lieu of direct age estimates from stellar physics, a possible alternate route for identifying ancient stars at intermediate metallicity is to appeal to specific metal-producing populations (e.g. *r*-process in core collapse SNe) that are likely to have occurred before other high-yield populations (e.g. *s*-process in AGBs, Fe peak elements in SNe Ia). While the precise origin of the *r*-process continues to be controversial (Winteler et al. 2012; Arcones & Thielemann 2013), with recent work suggesting a prompt channel in neutron star mergers (Belczynski et al. 2017), most models suggest that *r*-process enhancement with respect to Fe peak and *s*-process elements provides strong evidence a star is ancient (Frebel & Norris 2015).

Are there stars at [Fe/H] ~ -2 that have enhanced *r*-process elements compared to *s*-process elements? The literature is sparse, but some candidates do exist. A newly revealed example is the retrograde halo star RAVE J153830.9-180424 with [Fe/H] = −2.09, enhanced [α/Fe] = 0.34, enhanced [Eu/Fe] = 1.27, and suppressed [Ba/Fe] (Sakari et al. 2018). Detailed modelling of the actinide elements (Th, U) with respect to the other heavy elements supports the idea of this star being ancient, albeit with systematic uncertainties of several Gyr. Similar abundance patterns have also been found for some stars in metal-poor GCs (Sneden et al. 1997; Worley et al. 2013; Roederer & Thompson 2015).

Indeed, although their formation remains poorly understood theoretically, GC age constraints purely from stellar models are consistent with a large fraction of metal-poor GCs forming before $z = 5$ (Chaboyer 1995; Krauss & Chaboyer 2003; Bastian & Lardo 2017). Because GCs are too small to be properly resolved in the simulations we study here, we cannot yet predict their ages and $z = 0$ spatial distribution a priori. Dynamical friction arguments (e.g. Capuzzo-Dolcetta 1993; Carlberg 2017) suggest that since-disrupted GCs should be found in the inner bulge, and recent observations appear to support this idea (Minniti et al. 2016; Schiavon et al. 2017). Modelling the self-consistent formation and evolution of GCs in a cosmological context is a promising avenue for future work.

Given the nature and extent of existing stellar surveys and the difficulty of reliably age-dating old stars, it is unsurprising that metal-enriched ancient stars are yet to be identified in significant numbers. If such stars *can* be reliably identified in the future, then their spatial distribution will serve as a constraint on feedback models: because these stars were formed when the MW's progenitor's shallow potential was more susceptible to feedback-driven outflows than at late times, the dynamical imprint of baryon-driven potential fluctuations in our simulations is much larger for ancient stars than for stars formed at late times.

REFERENCES

Abel T., Bryan G. L., Norman M. L., 2000, ApJ, 540, 39
Aguado D. S., Allende Prieto C., González Hernández J. I., Rebolo R., 2018, ApJ, 854, L34
Anglés-Alcázar D., Faucher-Giguère C.-A., Kereš D., Hopkins P. F., Quataert E., Murray N., 2017, MNRAS, 470, 4698
Arcones A., Thielemann F.-K., 2013, J. Phys. G Nucl. Phys., 40, 013201
Árnadóttir A. S., Feltzing S., Lundström I., 2010, A&A, 521, A40
Asplund M., Grevesse N., Sauval A. J., Scott P., 2009, ARA&A, 47, 481
Astropy Collaboration, 2013, A&A, 558, A33
Baade W., 1946, PASP, 58, 249
Baade W., 1951, Publ. Michigan Obs., 10, 7
Bailey J. E. et al., 2015, Nature, 517, 56
Baker M., Willman B., 2015, AJ, 150, 160
Bastian N., Lardo C., 2017, preprint (arXiv:1712.01286)
Beers T. C., Christlieb N., 2005, ARA&A, 43, 531
Beers T. C., Preston G. W., Shectman S. A., 1985, AJ, 90, 2089
Belczynski K. et al., 2017, preprint (arXiv:1712.00632)
Beniamini P., Dvorkin I., Silk J., 2018, MNRAS, in press
Bessell M. S. et al., 2015, ApJ, 806, L16
Bland-Hawthorn J., Peebles P. J. E., 2006, Science, 313, 311
Bland-Hawthorn J., Sutherland R., Webster D., 2015, ApJ, 807, 154
Blumenthal G. R., Faber S. M., Flores R., Primack J. R., 1986, ApJ, 301, 27
Bonaca A., Conroy C., Wetzel A., Hopkins P. F., Kereš D., 2017, ApJ, 845, 101
Bovill M. S., Ricotti M., 2011, ApJ, 741, 17
Bromm V., 2013, Rep. Prog. Phys., 76, 112901
Bromm V., Larson R. B., 2004, ARA&A, 42, 79
Bromm V., Yoshida N., 2011, ARA&A, 49, 373
Brook C. B., Kawata D., Scannapieco E., Martel H., Gibson B. K., 2007, ApJ, 661, 10
Brown T. M. et al., 2014, ApJ, 796, 91
Bullock J. S., Johnston K. V., 2005, ApJ, 635, 931
Bullock J. S., Kravtsov A. V., Weinberg D. H., 2001, ApJ, 548, 33
Capuzzo-Dolcetta R., 1993, ApJ, 415, 616
Carlberg R. G., 2017, ApJ, 861, 69
Casey A. R., Schlaufman K. C., 2015, ApJ, 809, 110

Cayrel R. et al., 2001, Nature, 409, 691
Cescutti G., Chiappini C., Hirschi R., 2017, preprint (arXiv:1710.11014)
Chaboyer B., 1995, ApJ, 444, L9
Chaboyer B. et al., 2017, ApJ, 835, 152
Chan T. K., Kereš D., Oñorbe J., Hopkins P. F., Muratov A. L., Faucher-Giguère C.-A., Quataert E., 2015, MNRAS, 454, 2981
Chaplin W. J. et al., 2014, ApJS, 210, 1
Chiavassa A., Casagrande L., Collet R., Magic Z., Bigot L., Thevenin F., Asplund M., 2018, A&A, 611, A11
Choi J., Dotter A., Conroy C., Cantiello M., Paxton B., Johnson B. D., 2016, ApJ, 823, 102
Choksi N., Gnedin O., Li H., 2018, preprint (arXiv:1801.03515)
Christlieb N., 2003, in Schielicke R. E., ed., Reviews in Modern Astronomy. Wiley, New York. p. 191
Christlieb N. et al., 2002, Nature, 419, 904
Cooper A. P., Parry O. H., Lowing B., Cole S., Frenk C., 2015, MNRAS, 454, 3185
Cooper A. P. et al., 2010, MNRAS, 406, 744
Corlies L., Johnston K. V., Tumlinson J., Bryan G., 2013, ApJ, 773, 105
De Silva G. M. et al., 2015, MNRAS, 449, 2604
Di Cintio A., Brook C. B., Macciò A. V., Stinson G. S., Knebe A., Dutton A. A., Wadsley J., 2014, MNRAS, 437, 415
Eggen O. J., Lynden-Bell D., Sandage A. R., 1962, ApJ, 136, 748
El-Badry K., Weisz D. R., Quataert E., 2017a, MNRAS, 468, 319
El-Badry K., Wetzel A., Geha M., Hopkins P. F., Kereš D., Chan T. K., Faucher-Giguère C.-A., 2016, ApJ, 820, 131
El-Badry K., Wetzel A. R., Geha M., Quataert E., Hopkins P. F., Kereš D., Chan T. K., Faucher-Giguère C.-A., 2017b, ApJ, 835, 193
El-Badry K. et al., 2018a, MNRAS, 477, 1536
El-Badry K. et al., 2018b, MNRAS, 473, 1930
Elias L. M., Sales L. V., Creasey P., Cooper M. C., Bullock J. S., Rich M. R., Hernquist L., 2018, MNRAS, 479, 4004
Epstein C. R. et al., 2014, ApJ, 785, L28
Escala I. et al., 2018, MNRAS, 474, 2194
Faucher-Giguère C.-A., 2018, MNRAS, 473, 3717
Feltzing S. et al., 2017, preprint (arXiv:1708.08884)
Fernández-Alvar E. et al., 2017, MNRAS, 465, 1586
Fitts A. et al., 2018, MNRAS, 479, 319
Fouesneau M., Rix H.-W., von Hippel T., Hogg D. W., Tian H., 2018, preprint (arXiv:1802.06663)
Frebel A., Christlieb N., Norris J. E., Thom C., Beers T. C., Rhee J., 2007, ApJ, 660, L117
Frebel A., Norris J. E., 2015, ARA&A, 53, 631
Freeman K., Bland-Hawthorn J., 2002, ARA&A, 40, 487
Gao L., Theuns T., Frenk C. S., Jenkins A., Helly J. C., Navarro J., Springel V., White S. D. M., 2010, MNRAS, 403, 1283
García Pérez A. E. et al., 2013, ApJ, 767, L9
Garrison-Kimmel S. et al., 2017a, preprint (arXiv:1712.03966)
Garrison-Kimmel S. et al., 2017b, MNRAS, 471, 1709
Garrison-Kimmel S. et al., 2018, preprint (arXiv:1806.04143)
Griffen B. F., Dooley G. A., Ji A. P., O'Shea B. W., Gómez F. A., Frebel A., 2018, MNRAS, 474, 443
Hansen T. T. et al., 2017, ApJ, 838, 44
Harris W. E., 1996, AJ, 112, 1487
Helmi A., 2008, A&A Rev., 15, 145
Helmi A. et al., 2003, ApJ, 586, 195
Hill V., Christlieb N., Beers T. C., Barklem P. S., Kratz K.-L., Nordström B., Pfeiffer B., Farouqi K., 2017, A&A, 607, A91
Hill V. et al., 2002, A&A, 387, 560
Hopkins P. F., 2015, MNRAS, 450, 53
Hopkins P. F., Kereš D., Oñorbe J., Faucher-Giguère C.-A., Quataert E., Murray N., Bullock J. S., 2014, MNRAS, 445, 581
Hopkins P. F. et al., 2017a, MNRAS, in press
Hopkins P. F. et al., 2017b, MNRAS, 477, 1578
Howes L. M. et al., 2015, Nature, 527, 484
Howes L. M. et al., 2016, MNRAS, 460, 884
Hunter J. D., 2007, Comput. Sci. Eng., 9, 90

Ishiyama T., Sudo K., Yokoi S., Hasegawa K., Tominaga N., Susa H., 2016, ApJ, 826, 9

Ivezić Ž. et al., 2008, ApJ, 684, 287

Ji A. P., Frebel A., 2018, ApJ, 856 , 138

Ji A. P., Frebel A., Chiti A., Simon J. D., 2016, Nature, 531, 610

Johnston K. V., Bullock J. S., Sharma S., Font A., Robertson B. E., Leitner S. N., 2008, ApJ, 689, 936

Joyce M., Chaboyer B., 2017, ApJ , 856, 10

Karlsson T., Bromm V., Bland-Hawthorn J., 2013, Rev. Mod. Phys., 85, 809

Keller S. C. et al., 2014, Nature, 506, 463

Kirby E. N., Simon J. D., Geha M., Guhathakurta P., Frebel A., 2008, ApJ, 685, L43

Komiya Y., Habe A., Suda T., Fujimoto M. Y., 2010, ApJ, 717, 542

Krauss L. M., Chaboyer B., 2003, Science, 299, 65

Kroupa P., 2001, MNRAS, 322, 231

Kunder A. et al., 2017, AJ, 153, 75

Lamberts A. et al., 2018, preprint (arXiv:1801.03099)

Li H.-N., Zhao G., Christlieb N., Wang L., Wang W., Zhang Y., Hou Y., Yuan H., 2015, ApJ, 798, 110

Magg M., Hartwig T., Agarwal B., Frebel A., Glover S. C. O., Griffen B. F., Klessen R. S., 2018, MNRAS, 473, 5308

Majewski S. R. et al., 2017, AJ, 154, 94

Ma X., Hopkins P. F., Faucher-Giguère C.-A., Zolman N., Muratov A. L., Kereš D., Quataert E., 2016, MNRAS, 456, 2140

Ma X., Hopkins P. F., Wetzel A. R., Kirby E. N., Anglés-Alcázar D., Faucher-Giguère C.-A., Kereš D., Quataert E., 2017, MNRAS, 467, 2430

Maxwell A. J., Wadsley J., Couchman H. M. P., Mashchenko S., 2012, ApJ, 755, L35

McKee C. F., Tan J. C., 2008, ApJ, 681, 771

Miglio A. et al., 2012, MNRAS, 419, 2077

Minniti D., Contreras Ramos R., Zoccali M., Rejkuba M., Gonzalez O. A., Valenti E., Gran F., 2016, ApJ, 830, L14

Ness M., Hogg D. W., Rix H.-W., Martig M., Pinsonneault M. H., Ho A. Y. Q., 2016, ApJ, 823, 114

Nissen P. E., Silva Aguirre V., Christensen-Dalsgaard J., Collet R., Grundahl F., Slumstrup D., 2017, A&A, 608, A112

Norris J. E. et al., 2013, ApJ, 762, 28

Oluseyi H. M. et al., 2012, AJ, 144, 9

Oman K. A. et al., 2015, MNRAS, 452, 3650

Oñorbe J., Boylan-Kolchin M., Bullock J. S., Hopkins P. F., Kereš D., Faucher-Giguère C.-A., Quataert E., Murray N., 2015, MNRAS, 454, 2092

Pontzen A., Governato F., 2012, MNRAS, 421, 3464

Pontzen A., Governato F., 2014, Nature, 506, 171

Power C., Navarro J. F., Jenkins A., Frenk C. S., White S. D. M., Springel V., Stadel J., Quinn T., 2003, MNRAS, 338, 14

Purcell C. W., Bullock J. S., Kazantzidis S., 2010, MNRAS, 404, 1711

Rauer H. et al., 2014, Exp. Astron., 38, 249

Read J. I., Gilmore G., 2005, MNRAS, 356, 107

Ricker G. R. et al., 2015, J. Astron. Telesc. Instrum. Syst., 1, 014003

Robin A. C. et al., 2012, A&A, 543, A100

Roederer I. U., Thompson I. B., 2015, MNRAS, 449, 3889

Sakari C. M. et al., 2018, ApJ, 854, L20

Salvadori S., Ferrara A., Schneider R., Scannapieco E., Kawata D., 2010, MNRAS, 401, L5

Salvadori S., Schneider R., Ferrara A., 2007, MNRAS, 381, 647

Sandage A., 1986, ARA&A, 24, 421

Sanderson R. E. et al., 2017, preprint (arXiv:1712.05808)

Sanderson R. E. et al., 2018, preprint (arXiv:1806.10564)

Sawala T. et al., 2016, MNRAS, 457, 1931

Scannapieco E., Kawata D., Brook C. B., Schneider R., Ferrara A., Gibson B. K., 2006, ApJ, 653, 285

Schiavon R. P. et al., 2017, MNRAS, 465, 501

Schlaufman K. C., Casey A. R., 2014, ApJ, 797, 13

Sharma M., Theuns T., Frenk C., 2017, MNRAS, 479, 1638

Sharma S. et al., 2018, MNRAS, 473, 2004

Sherwood V. E., Plaut L., 1975, Variable Stars and Stellar Evolution . Springer , Berlin

Silva Aguirre V. et al., 2015, MNRAS, 452, 2127

Sneden C., Kraft R. P., Shetrone M. D., Smith G. H., Langer G. E., Prosser C. F., 1997, AJ, 114, 1964

Sneden C., McWilliam A., Preston G. W., Cowan J. J., Burris D. L., Armosky B. J., 1996, ApJ, 467, 819

Soderblom D. R., 2010, ARA&A, 48, 581

Soszyński I. et al., 2011, Acta Astron., 61, 1

Sparre M., Hayward C. C., Feldmann R., Faucher-Giguère C.-A., Muratov A. L., Kereš D., Hopkins P. F., 2017, MNRAS, 466, 88

Starkenburg E., Oman K. A., Navarro J. F., Crain R. A., Fattahi A., Frenk C. S., Sawala T., Schaye J., 2017a, MNRAS, 465, 2212

Starkenburg E. et al., 2017b, MNRAS, 471, 2587

Stello D. et al., 2015, ApJ, 809, L3

Stinson G. S., Dalcanton J. J., Quinn T., Gogarten S. M., Kaufmann T., Wadsley J., 2009, MNRAS, 395, 1455

Strömgren B., 1963, QJRAS, 4, 8

Su K.-Y., Hopkins P. F., Hayward C. C., Faucher-Giguère C.-A., Kereš D., Ma X., Robles V. H., 2017, MNRAS, 471, 144

Tornatore L., Ferrara A., Schneider R., 2007, MNRAS, 382, 945

Trenti M., Stiavelli M., Michael Shull J., 2009, ApJ, 700, 1672

Tumlinson J., 2010, ApJ, 708, 1398

Van Der Walt S., Colbert S. C., Varoquaux G., 2011, Comput. Sci. Eng. , 13

Walker A. R., Terndrup D. M., 1991, ApJ, 378, 119

Wallerstein G., 1962, ApJS, 6, 407

Wallerstein G., Greenstein J. L., Parker R., Helfer H. L., Aller L. H., 1963, ApJ, 137, 280

Wetzel A. R., Hopkins P. F., Kim J.-h., Faucher-Giguère C.-A., Kereš D., Quataert E., 2016, ApJ, 827, L23

White S. D. M., Springel V., 2000, in Weiss A., Abel T. G., Hill V., eds, The First Stars. Springer , Berlin, p. 327

Winteler C., Käppeli R., Perego A., Arcones A., Vasset N., Nishimura N., Liebendörfer M., Thielemann F.-K., 2012, ApJ, 750, L22

Wise J. H., Turk M. J., Norman M. L., Abel T., 2012, ApJ, 745, 50

Worley C. C., Hill V., Sobeck J., Carretta E., 2013, A&A, 553, A47

Yong D. et al., 2013, ApJ, 762, 26

Youakim K. et al., 2017, MNRAS, 472, 2963

APPENDIX A: EFFECT OF DIFFUSION COEFFICIENT AND RESOLUTION

Fig. A1 shows the effect of varying the simulation mass resolution (top panel) and the turbulent diffusion coefficient (bottom panel). The quantity plotted is the fraction of stars within 10 kpc of the solar neighbourhood with [Fe/H] < −2 that formed before a given redshift, identical to the right-hand panel of Fig.2. We compare three different versions of the m12i simulation. The fiducial version analysed throughout text (black line) has a baryon mass resolution of $m_b = 7070 M_\odot$ and uses a diffusion coefficient $C_0 \approx 0.003$ (see Hopkins et al. 2017a for details).

In the top panel, we compare this run to one with eight times lower mass resolution ($m_b = 56600 M_\odot$) and the same diffusion coefficient and critical density for star formation as the fiducial run. For stars formed after $z \sim 7$, the fraction of metal-poor stars that formed before a given redshift agrees between the two resolution levels within ~20 per cent. At higher z_{form}, the predictions of the two resolution levels disagree more significantly, with a maximum discrepancy of a factor of 5. The fraction of metal-poor stars that are very old is higher in the lower resolution run. We find that the total age distribution of ancient stars is similar in the high- and low-resolution runs. Typical metallicities of the most ancient stars are higher in the high-resolution run, indicating that gas is enriched somewhat more rapidly at high resolution.

The bottom panel compares two runs with the same mass resolution ($m_b = 56600 M_\odot$) and different diffusion coefficients. The red dashed line is the same as in the top panel, while the blue line
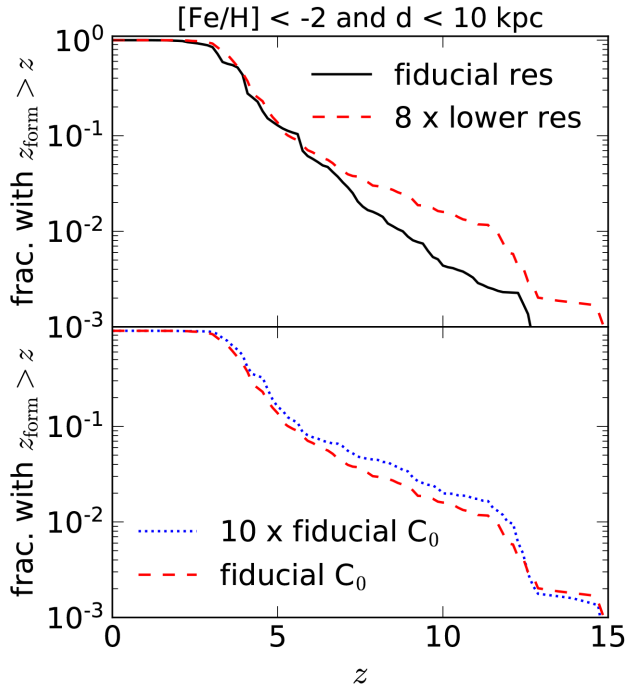
Figure A1. Effect of varying the mass resolution (top) and diffusion coefficient (bottom) on the fraction of metal-poor stars that formed before a particular redshift. The black line shows the default m12i simulation, identical to the black line in the right-hand panel of Fig.2. The red dashed line shows the same simulation run with eight times lower mass resolution but the same diffusion coefficient. The blue dotted line shows a run with eight times lower mass resolution than the default m12i and 10 times higher diffusion coefficient.

has a diffusion coefficient that is 10 times larger. Consistent with Escala et al. (2018), we find that the simulation predictions are not very sensitive to the choice of diffusion coefficient: the fraction of metal-poor stars that formed before a given z always agrees within ± 50 per cent across the two simulations. We also find that the two simulations' stellar metallicity distributions (Fig. 3) are in good agreement at all redshifts.

This paper has been typeset from a TEX/LATEX file prepared by the author.